International Journal of Bifurcation and Chaos, Vol. 27, No. 6 (2017) 1750082 (32 pages)

DOI: 10.1142/S0218127417500821

Glider Collisions in Hybrid Cellular Automaton with Memory Rule(43, 74)

Bo Chen* and Fangyue Chen†
Department of Mathematics, School of Science,
Hangzhou Dianzi University, Hangzhou,
Zhejiang 310018, P. R. China
**chenbo4068922@126.com*
†*fychen@hdu.edu.cn*

Genaro J. Martínez
Escuela Superior de Cómputo,
Instituto Politécnico Nacional, México D.F., México
International Center of Unconventional Computing,
University of the West of England, BS16 1QY Bristol, UK
Genaro.Martinez@uwe.ac.uk

Received June 7, 2016

In the case of one-dimensional cellular automaton (CA), a hybrid CA (HCA) is the member whose evolution of the cells is dependent on nonunique global functions. The HCAs exhibit a wide range of traveling and stationary localizations in their evolution. We focus on HCA with memory (HCAM) because they produce a host of gliders and complicated glider collisions by introducing the hybrid mechanism. In particular, we undertake an exhaustive search of gliders and describe their collisions using quantitative approach in HCAM(43, 74). By introducing the symbol vector space and exploiting the mathematical definition of HCAM, we present an analytical method of complex asymptotic dynamics of the gliders.

Keywords: Hybrid cellular automata with memory; glider; collisions; symbolic dynamics; directed graph representation; transition matrix; chaos.

1. Introduction

Cellular automata (CAs) are dynamical systems discrete in time and space: the next state of each cell depends solely on its current neighborhood configuration [Von-Neumann, 1966]. One of the most interesting subjects about CAs is that a kaleidoscope of marvellous spatiotemporal patterns can continuously spring up from apparently simple rules. The patterns guide us on the trips into the depths of the field of the computing universe [Adamatzky & Martínez, 2016]. Significantly, elementary cellular automaton (ECA) is a one-dimensional array of finite automaton, each one has two states and updates its state in discrete time depending on its own state and states of its two closest neighbors synchronously [Wolfram, 1983, 1984, 1986]. Wolfram informally divided the 256 ECA rules into four classes using dynamical concepts — stability, periodicity, chaos and complexity [Wolfram, 2002]. Notably, it is worth mentioning that ECA rule 110, belonging to complexity, has been proved universal via simulating a cyclic tag system [Cook, 2004].

Conventional CAs are Markovian (ahistoric, memoryless for 1). In order to extend ECA rules, Alonso-Sanz originally proposed ECA with memory (ECAM), whose each output cell is allowed to remember its previous states during a certain fixed period of evolution [Alonso-Sanz & Martin, 2002, 2003, 2004, 2006]. The memory mechanism is roughly divided into embedded memory and delay memory, each of which can be subdivided into several types ulteriorly. For example, the work [Martínez *et al.*, 2013] explored three delay memory functions — majority, minority and parity. This way, any ECA class can be transformed to another ECA class — without changing the skeleton of cell-state transition function — and vice versa by just selecting an appropriate kind of memory. For instance, under particular majority memory functions, rule 30 and rule 126 are endowed with complex gliders phenomena. Their morphological complexity and glider dynamics are analyzed in [Martínez *et al.*, 2010a, 2010b] by mean field approximation, representation of tiles, basins of attraction, De Bruijn diagrams and so on. After classifying and coding the gliders, glider collisions are also explored in detail. In addition, there are many more research on CA with memory, see [Alonso-Sanz, 2013, 2016] and references therein.

Here, we briefly introduce the definitions of ECAM and hybrid CA (HCA). Each ECAM rule is composed of the memory function and the original ECA rule. In particular, for the memory function in [Chen *et al.*, 2015], the number of cells performing memory is three ($\tau = 3$); that is, the memory values are determined by the last three states of each cell. Furthermore, we regard minority memory as a function, which implies the ability of recording the values that have the minimum number of the corresponding last three states of each cell. For the cells at the moment, a row of memory values can be calculated. Then, the row of cell states at the next moment can be obtained via implementing the original ECA rule. On the other hand, in the case of one-dimensional CA, when the evolution of every single cell is only dependent on the unique global function, the CA is called uniform, otherwise it is called hybrid. Denoted by HCA(N, M), HCA rule composed of ECA rule N and ECA rule M, is specified to obey the ECA rule N at odd sites of the cell array and obey the rule M at even sites of the cell array [Cattell & Muzio, 1996; Bingham & Bingham, 2007]. Although the simple rules of HCA act on the same square tile structures, HCA may exhibit complex dynamical behaviors through local interactions.

Let the memory function ($\tau = 3$) be a concrete ECA rule, this paper conceives a particular extended ECAM model — hybrid cellular automata with memory (HCAM). One interesting question is whether the complicated dynamical behaviors can be captured in HCAM rules. Based on large amount of computer simulations and empirical observations, we list a multitude of HCAM rules of newfound and strong nonlinear spatiotemporal patterns.

In particular, though ECA rule 43 and rule 74 have simple evolution patterns respectively, HCAM$(43, 74)$ sparks off a series of different gliders and collisions because of the interaction of two local rules. In general, gliders are localized structures of nonquiescent and nonether patterns (ether represents a periodic background) translating along the automaton's lattice. Importantly, as gilders are crucial components of conception and simulation of the universal computing model, the concrete rules with a great variety of gliders have captured special attention in a series of CA research work [Martínez *et al.*, 2010a; Cook, 2004; Freire & Gallas, 2007; Chen *et al.*, 2012; Martínez *et al.*, 2014]. It leads to an intriguing possibility: HCAM$(43, 74)$ is an ideal candidate for the universal computing. In this paper, we are devoted to expanding an analytical characterization of symbolic dynamics analysis of the gliders with the HCAM rules.

The rest of this article is organized as follows: Section 2 presents several definitions of HCAM rules and introduces the HCAM$(43, 74)$. After classifying and coding the gliders in HCAM$(43, 74)$, the collision formula are depicted in Sec. 3 through ether and glider factors. Furthermore, by introducing the symbol vector space and exploiting the mathematical definition of HCAMs, Sec. 4 investigates in detail the dynamical properties of glider f by directed graph representation and transition matrix in the framework of symbolic dynamics. It is worth mentioning that the method is easy to apply to all other gliders in HCAM$(43, 74)$ or different HCAM rules. Finally, Sec. 5 highlights the main results.

HCAM(35,133)

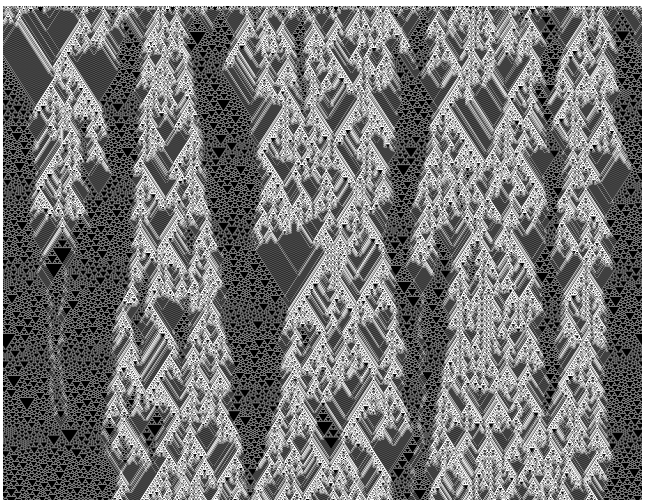

HCAM(37,29)

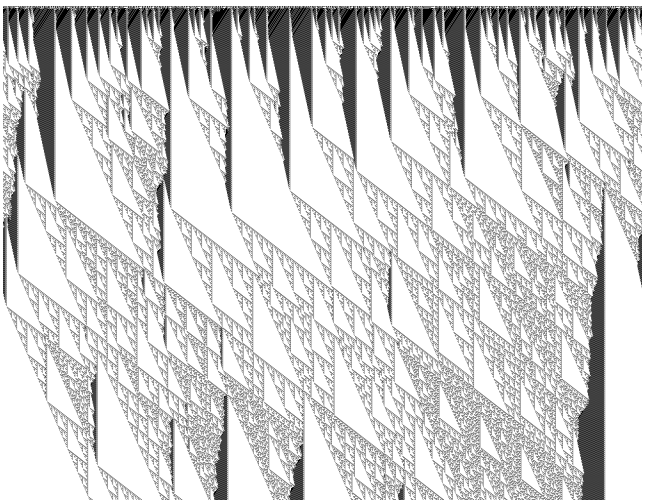

HCAM(38,22)

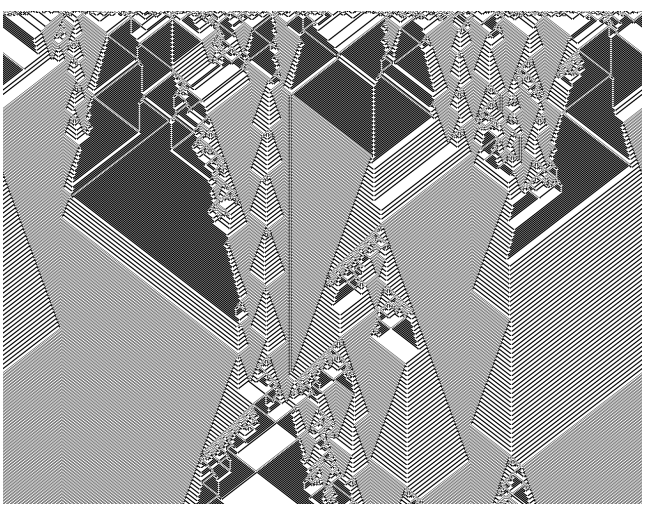

HCAM(43,74)

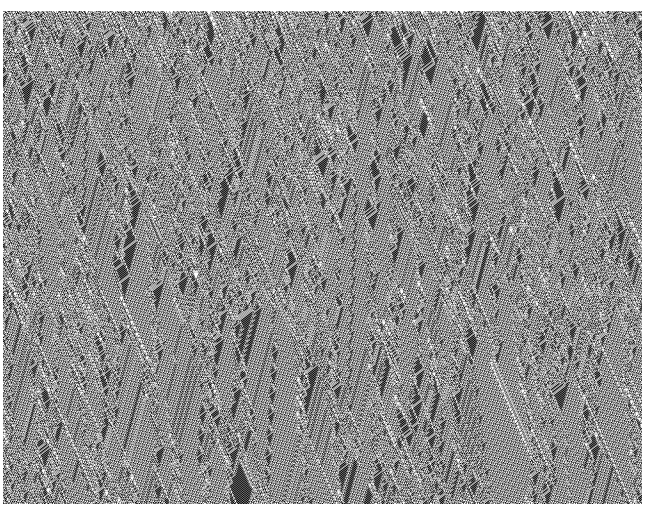

HCAM(104,54)

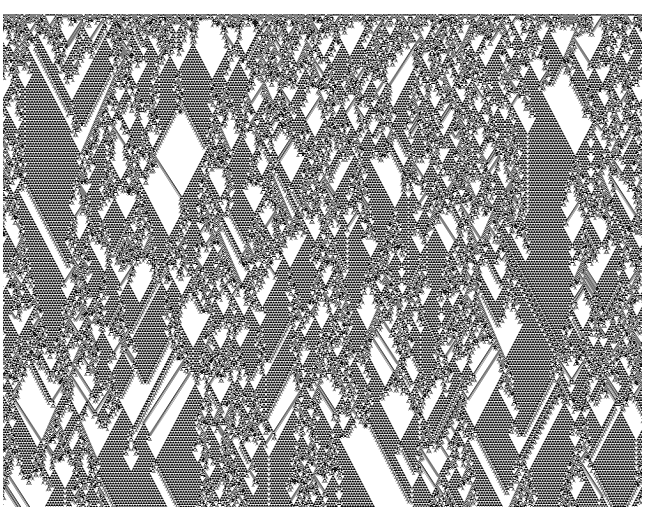

HCAM(134,110)

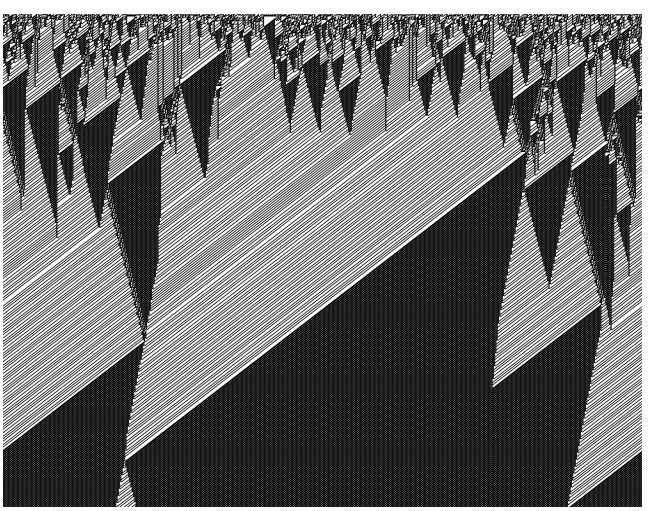

Fig. 1. The newfound spatiotemporal patterns of several HCAM rules.

2. The Introduction of HCAM(43, 74)

First and foremost, following [Zhou, 1997; Kitchens, 1998], several terminology and notations are the necessary prerequisites to the rigorous consideration of this subject. The set of biinfinite configurations is denoted by $S^Z = \cdots S \times S \times S \cdots$ and a metric d on S^Z is defined as

$$d(x, \overline{x}) = \sum_{i=-\infty}^{+\infty} \frac{1}{2^{|i|}} \frac{\tilde{d}(x_i, \overline{x}_i)}{1 + \tilde{d}(x_i, \overline{x}_i)},$$

where $S = \{0, 1, \ldots, k-1\}$, $x, \overline{x} \in S^Z$ and $\tilde{d}(\cdot, \cdot)$ is the metric on S defined as $\tilde{d}(x_i, \overline{x}_i) = 0$, if $x_i = \overline{x}_i$; otherwise, $\tilde{d}(x_i, \overline{x}_i) = 1$. The classical right-shift map σ is defined by $[\sigma(x)]_i = x_{i-1}$ for any $x \in S^Z$, $i \in Z$. A map $F : S^Z \to S^Z$ is a CA if and only if it is continuous and commutes with σ, i.e. $\sigma \circ F = F \circ \sigma$. For any CA, there exists a radius $r \geq 0$ and a local rule $N : S^{2r+1} \to S$ such that $[F(x)]_i = N(x_{[i-r,i+r]})$. Moreover, (S^Z, F) is a compact dynamical system.

According to the definition of ECAM [Alonso-Sanz & Martin, 2003; Martínez *et al.*, 2013], a memory function ϕ is implemented as follows: $s_i^{(t)} = \phi_i(x_i^{(t-\tau+1)}, \ldots, x_i^{(t-1)}, x_i^{(t)})^T$, where $1 \leq \tau \leq t$ determines the degree of memory and ϕ_i denotes the ith symbol of global memory function ϕ. Thus, $\tau = 1$ means conventional evolution, whereas $\tau = t$ means unlimited trailing memory. Each cell trait $s_i \in S$ is a state function of the states of cell i with memory backward up to the value τ. The memory implementation selected in this analysis commences to act as soon as t reaches the τ time-step. Initially, i.e. $t < \tau$, the automaton evolves in the conventional way. Furthermore, the original rule is applied on the cell states s to get an evolution with memory as: $[f(\cdots, s_{i-1}^{(t)}, s_i^{(t)}, s_{i+1}^{(t)}, \cdots)]_i = x_i^{(t+1)}$. In particular, the simplified expression of F is $f \circ \phi(x^{(t-\tau+1)}, \ldots, x^{(t-1)}, x^{(t)})^T = x^{(t+1)}$, where $x^{(t+k)} = (\cdots, x_{i-1}^{(t+k)}, x_i^{(t+k)}, x_{i+1}^{(t+k)}, \cdots)$, $k = -\tau + 1, \ldots, -1, 0, 1$.

As is to be expected, if we set the memory function as a concrete ECA rule, a kind of hybrid CA evolution function will be composed of a pair of ECA rules. Denoted by HCAM(N, M), a hybrid CA rule is composed of ECA rule N and ECA rule M, which is specified to obey the ECA rule N in the vertical direction — $s_i^{(t)} = [f_N(x_i^{t-2}, x_i^{t-1}, x_i^t)^T]_i$ and obey the rule M in the horizontal direction — $x_i^{(t+1)} = [f_M(\cdots, s_{i-1}^{(t)}, s_i^{(t)}, s_{i+1}^{(t)}, \cdots)]_i$. Then, the dynamical behavior of ECA rule M will also be changed in a subtle way. A schematic diagram of HCAM rule is provided in Fig. 2.

The spatiotemporal patterns of HCAM(43, 74) are displayed in Fig. 3. It is noted that all patterns

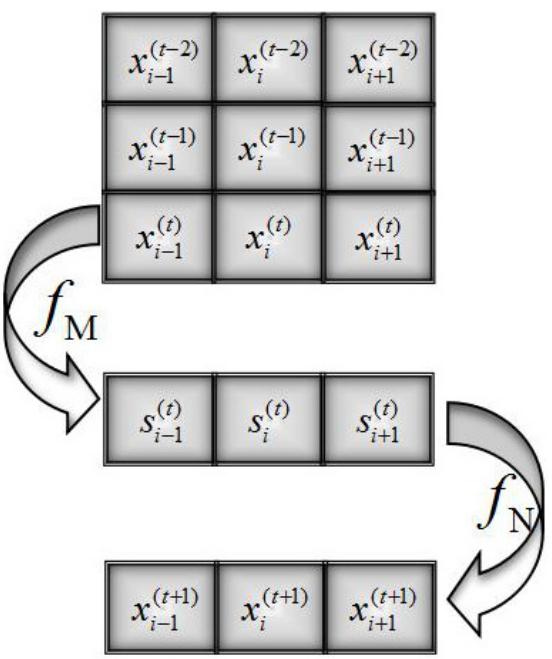

The Boolean truth table

	$[f_{43}]_i$	$[f_{74}]_i$
000	1	0
001	1	1
010	0	0
011	1	1
100	0	0
101	1	0
110	0	1
111	0	0

Fig. 2. The schematic diagram of HCAM(43, 74).

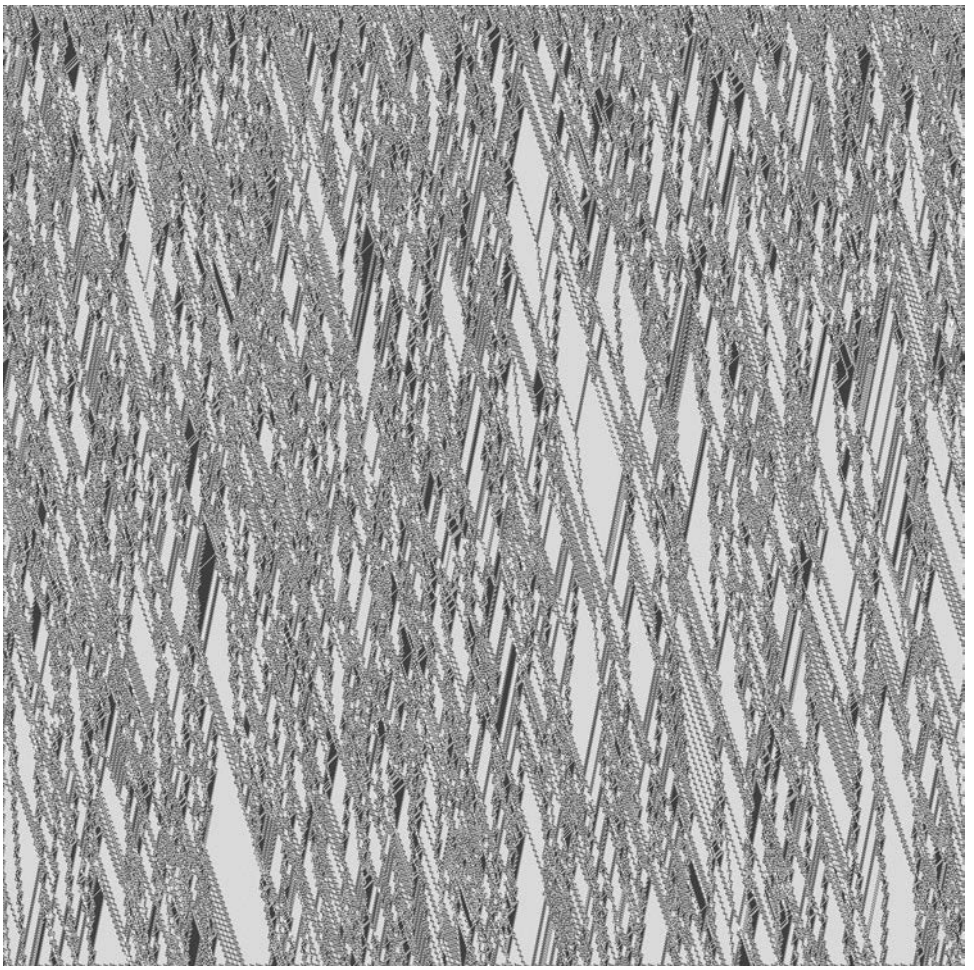

Fig. 3. Spatiotemporal pattern of HCA(168, 133), where white pixels are cells with state 0, and black pixels are cells with state 1 except the background of ether.

in this paper are studied under the periodic boundary condition. By designing a single filter of ether, the gliders are easy to be distinguished from each other.

Here, several computer experiment methods — Hamming distance, Jaccard distance, and Lameray diagram — are applied to explore the complexity of dynamical evolution process of three configurations in HCAM(43, 74). We compute the Hamming distance and Jaccard distance of each adjacent states, then draw the simulation diagrams according to the data.

Given two states in chronological order $x^{(t)}$ and $x^{(t+1)}$, each with n cells, the Jaccard coefficient is a useful measure of the overlap that $x^{(t)}$ and $x^{(t+1)}$ share with their states. Each attribute of $x^{(t)}$ and $x^{(t+1)}$ can either be 0 or 1. The total number of each combination of cells for both $x^{(t)}$ and $x^{(t+1)}$ are specified as follows: n_{11} represents the total number of cells where $x^{(t)}$ and $x^{(t+1)}$ both have the value of 1; n_{01} represents the total number of cells where the attribute of $x^{(t)}$ is 0 and the attribute of $x^{(t+1)}$ is 1; n_{10} represents the total number of cells where the attribute of $x^{(t)}$ is 1 and the attribute of $x^{(t+1)}$ is 0; n_{00} represents the total number of cells where $x^{(t)}$ and $x^{(t+1)}$ both have a value of 0. Each cell must fall into one of these four categories, meaning that $n_{11} + n_{01} + n_{10} + n_{00} = n$. The Jaccard similarity coefficient, J, is given as $J = n_{11}/(n_{01} + n_{10} + n_{11})$. The Jaccard distance, d_J, is given as $d_J = (M_{01} + M_{10})/(M_{01} + M_{10} + M_{11}) = 1 - J$.

The Hamming distance between $x^{(t)}$ and $x^{(t+1)}$, for the fixed length n, is the number of positions at which the corresponding symbols are different, which measures the minimum number of substitutions required to change $x^{(t)}$ into $x^{(t+1)}$. Furthermore, we standardize each distance value (divide n)

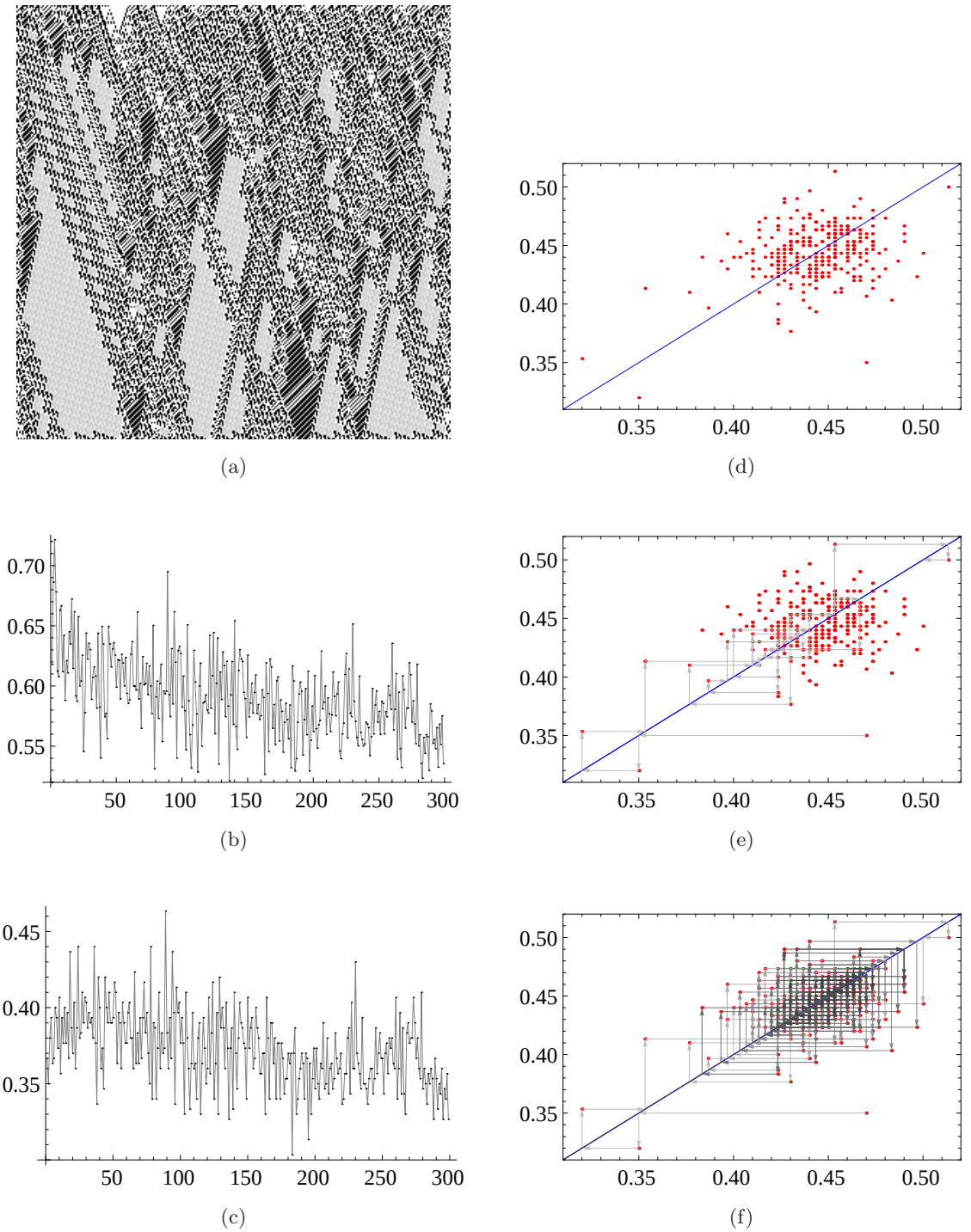

Fig. 4. (a) The spatiotemporal pattern of HCAM(43, 74) under random initial condition with 300 cells and 300 time steps, (b) the Jaccard distance diagram, (c) the Hamming distance diagram. At different measurement scales, the two diagrams show that there is no repeat of the states and present the random walk on the time series, (d) Lameray diagram without the cobweb, (e) Lameray diagram for first 50 iterations and (f) Lameray diagram for 300 iterations. The gray level of cobwebs is continuously deepening with steps. The cobwebs point to disordered directions subsequently. As is shown above, this implies the evolution of HCAM(43, 74) is unpredictable and complicated because of the gliders' collisions.

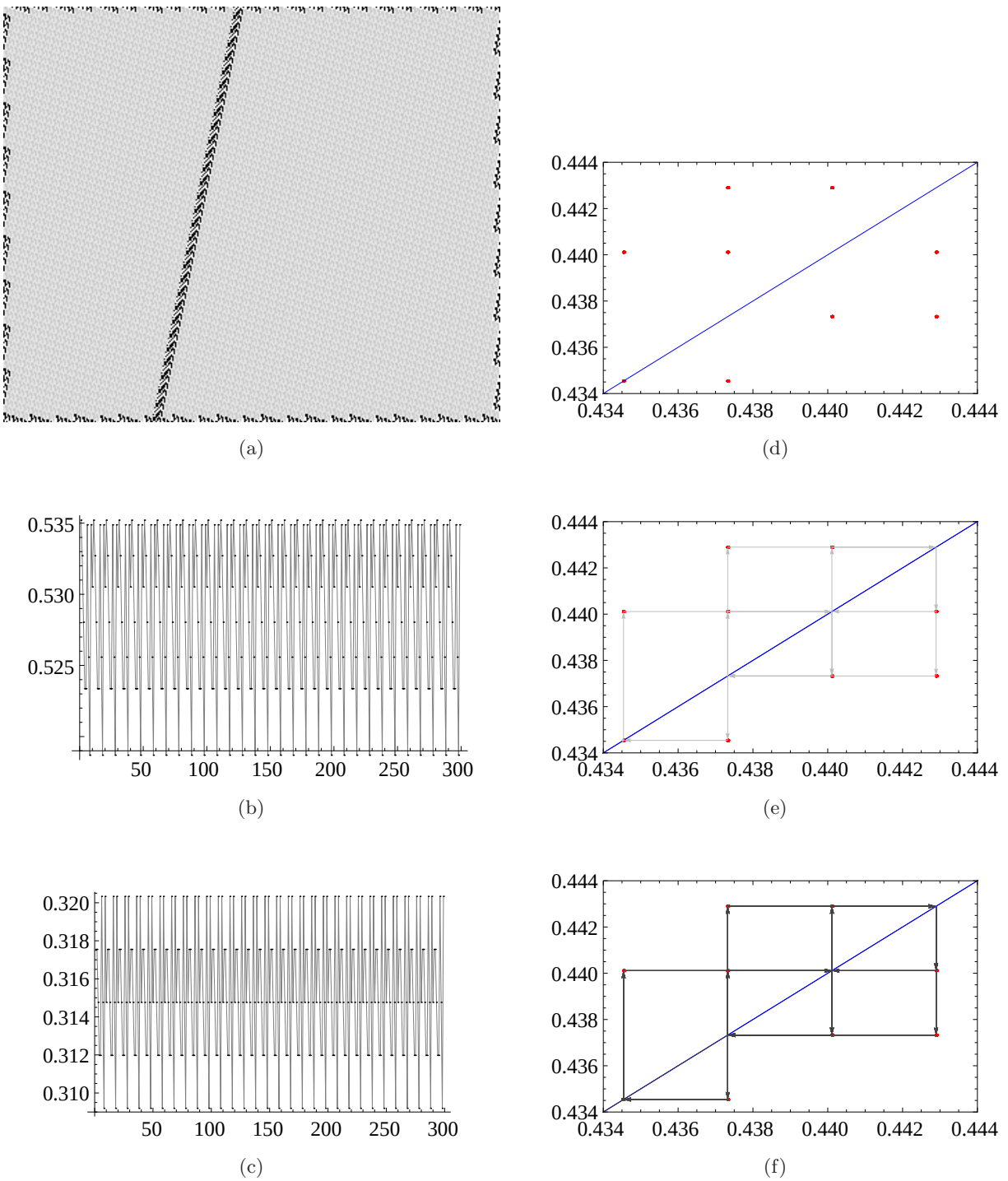

Fig. 5. (a) The spatiotemporal pattern of glider e with 359 cells and 300 time steps, (b) the Jaccard distance diagram, (c) the Hamming distance diagram. At different measurement scales, the two diagrams show that there is 10-periodic repeat of the states and presents regular evolution on the time series, (d) Lameray diagram without the cobweb, (e) Lameray diagram for first 50 iterations and (f) Lameray diagram for 300 iterations. The gray level of cobwebs is continuously deepening with steps. The cobwebs point to several permanent directions all the while. As is shown above, this implies the states of glider remain unchanged periodically.

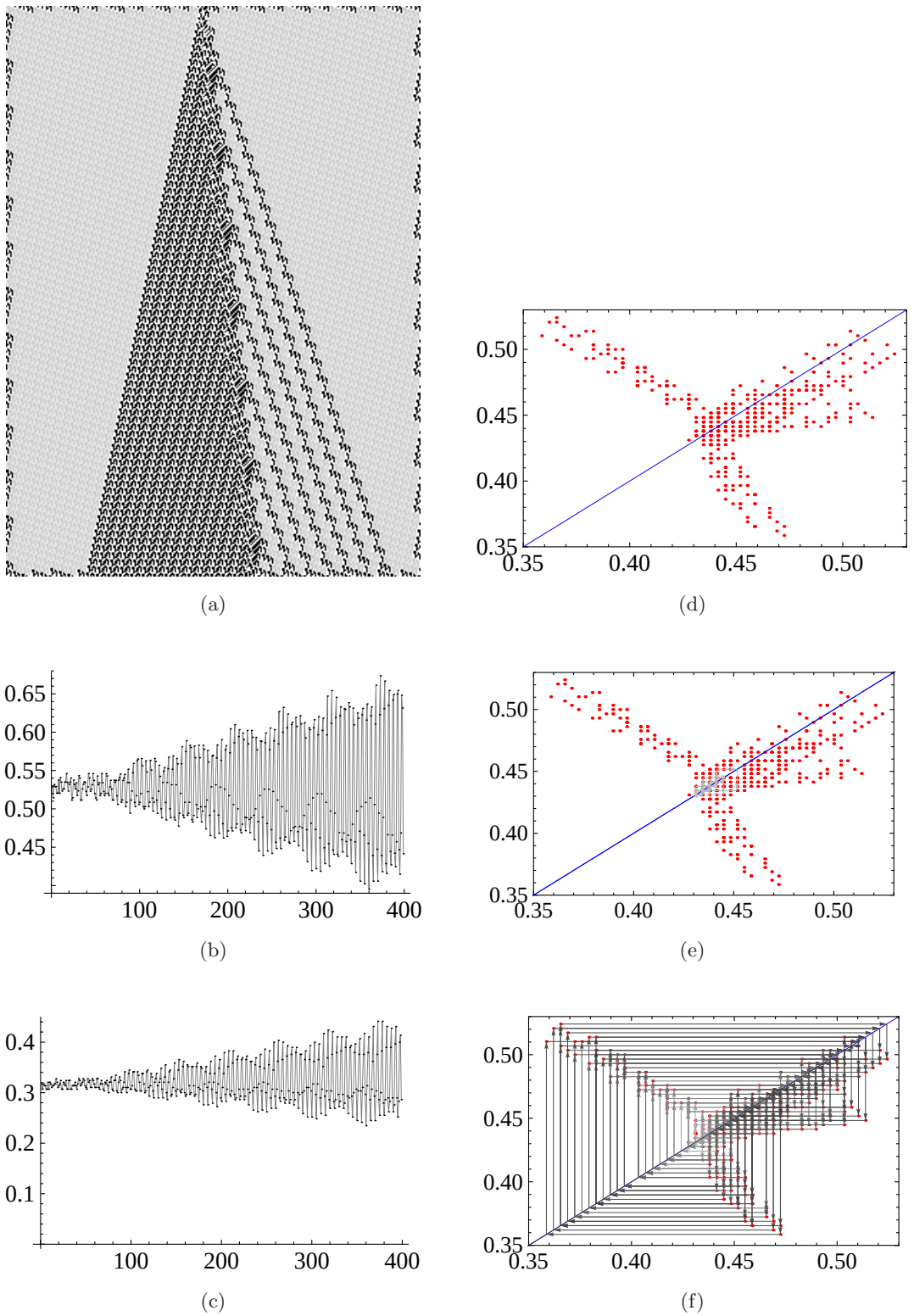

Fig. 6. (a) The spatiotemporal pattern of fusion with 290 cells and 400 time steps, (b) the Jaccard distance diagram, (c) the Hamming distance diagram. At different measurement scales, the two diagrams show that the distances are continued growth and the time series is an analogous oscillator whose fluctuating range is ever-increasing, (d) Lameray diagram without the cobweb, (e) Lameray diagram for first 50 iterations and (f) Lameray diagram for 400 iterations. The gray level of cobwebs is continuously deepening with steps. The cobweb's trajectory expands from the inside out. As is shown above, this implies the states of fusion are rhythmic and ceaselessly growing.

in order to better understand the data. For example, Hamming distance between 00100101 and 11100001 is 3/8.

An instructive way to analyze its dynamics is to plot the Lameray diagram starting from any generic initial point, and observe how its "cobweb" evolves from this initial point step by step. In [Chua *et al.*, 2005; Chua *et al.*, 2008], the equation of each state is the decimal equivalent of string $(x_0^t, \ldots, x_{n-1}^t)$ defined by

$$\phi_t = \sum_{i=0}^{I-1} x_i^t \cdot 3^{-(i+1)}.$$

However, we modify the equation to calculate the number of 1 in each string which is defined by

$$\phi_t = \sum_{i=0}^{I-1} x_i^t.$$

This change has less impact on the empirical observation.

3. Glider Collisions in HCAM(43, 74)

In order to gain further insights into the rich dynamics of HCAM(43, 74), we present a systematic analysis of computational glider behaviors in this section. A pair of types — original glider and composite glider — are classified and coded depending on dissimilar shift velocity and volumes. Every glider evolves under the uniform background of ether. We call the minimum component element of ether an *ether unit*. Thus, the background of ether in HCAM(43, 74) is composed of ether unit

$$\begin{pmatrix} 0 & 1 & 1 & & & \\ 0 & 1 & 1 & 0 & 1 & 0 \\ 0 & 0 & 1 & 0 & 1 & 1 \\ 0 & 0 & 1 & 1 & 0 & 1 \\ 0 & 0 & 1 & 0 & 0 & 1 \\ & & 0 & 0 & 0 & 1 \\ & & & & & 1 \end{pmatrix}.$$

Not all rows of the ether unit have six cells. In the process of ether matching, the remaining empty sites will be filled by the adjacent ether unit. And the whole background of ether can be obtained by splicing this ether unit repeatedly without any gap or overlap. To help visualize this, Fig. 7 provides a schematic diagram of ether matching according to the definition of tile in [Martínez *et al.*, 2014].

3.1. *Classification and codings of gliders*

Besides the ether unit, the shift configurations without arbitrary combination of diverse gliders are called *original gliders* (OGs). The OGs are the independent gliders which cannot be decomposed into

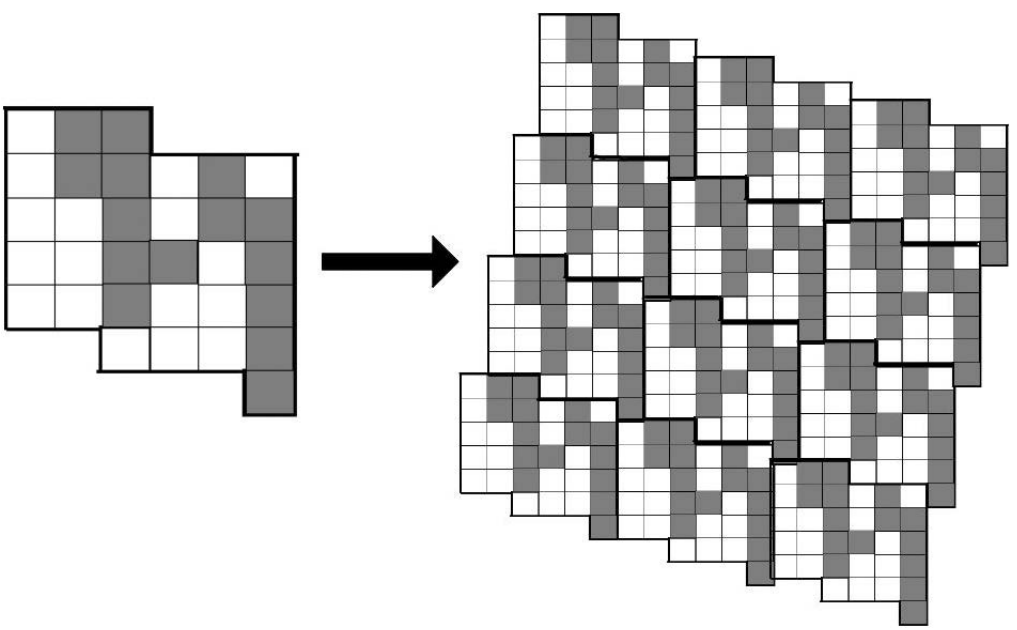

Fig. 7. The schematic diagram of ether matching, where white pixels are cells with state 0, and gray pixels are cells with state 1.

smaller ones. However, if several OGs have the same velocity, they will probably be assembled together and there are no ether units among them. These shift configurations are explicitly considered as the new gliders — *composite gliders* (CGs). In a survey of spatiotemporal patterns of HCA(168, 133), several OGs and CGs which have occurred frequently are recorded as different codings. The spatiotemporal patterns of 122 OGs and CGs are presented in this paper.

As different types of CGs can be assembled together by the same OG, we introduce the following codings of CGs. Let ξ be a concrete label of OG.

(1) The ξ^n, $n = 1, 2, 3, \ldots$, and $\xi\xi\cdots\xi\xi$ stand for the glider which are composed of two or more same ξ in two ways. As an example, the gliders i^2 and ii are recognized as simple superposition of two OG i in two ways.
(2) The ${}^n\xi$, $n = 1, 2, 3, \ldots$, stand for the complicated variants of glider ξ (not the simple composite) according to "With".
(3) The $\xi_{\langle n\rangle}$, $n = 1, 2, 3, \ldots$, stand for the different complicated variants of glider ξ (not the simple composite) according to "With".

The spatiotemporal patterns of 66 OGs and CGs are illustrated in Fig. 8, and the others are placed in Appendix A. Since the evolution of HCAM(43, 74) is of high complexity and the collisions of different gliders can spark off new gliders, not all gliders are enumerated here. Table 1 presents the properties of gliders, where the "Gliders" column shows the labels of gliders, the "Velocity" column shows the shift features of gliders and the "With" column indicates maximal and minimal sizes of gliders. For any given glider, the velocity is calculated from its shift number divided by its period. The plus sign denotes that the glider shifts to right, and the minus sign denotes that the glider shifts to left. If a concrete glider is assembled together by the same OG, the "With" column also lists some examples which often appear in the patterns. By the way, the spatiotemporal patterns of three fusions are shown in Fig. 9.

In order to exploit the mathematical definition of collisions between two gliders in HCAM(43, 74), we perform a qualitative analysis of collision formulae via one-dimensional strings and introduce the *ether factor* and *glider factor*, which are denoted by E and $[\xi]$ respectively. Here, ξ is a concrete label of glider. Firstly, the ether factor

$$E = \begin{pmatrix} 0,1,1,0,0,0,1,0,0,1,1,0,1,0,1,1,0,1,0,0,0,0,1,0,0,1,0,0,1,0,1,1 \\ 0,1,1,0,1,0,0,0,0,1,0,0,1,0,0,1,0,1,1,0,1,1,0,0,0,1,0,0,1,1,0,1 \\ 0,0,1,0,1,1,0,1,1,0,0,0,1,0,0,1,1,0,1,0,1,1,0,1,0,0,0,0,1,0,0,1 \end{pmatrix}$$

is introduced according to the characterization of ether unit. For convenience, we introduce the abbreviations — $-(3527595590/2989920790/2427818420)$, where the integers are respectively decimal code expression of three lines string.

The ether factor is determined by the shift characteristic and width of ether unit. Then, the glider factor $[\xi]$ is introduced which refers to a row cell state of the glider ξ under the background of the ether. If the glider ξ has the period M, it has M different glider factors. For example, because the glider a has the period 5 according to Table 1, there are five glider factors and each one can produce the entire glider a after the evolution of five time steps. In general, for a pair of gliders ξ and η with different velocity, there are two scenarios: when particular kinds of glider factors $[\xi]$ and $[\eta]$ are chosen, the collision results are periodically variational owing to the different numbers of ether factor between $[\xi]$ and $[\eta]$. However, when the different kinds of glider factors $[\xi]'$ and $[\eta]'$ are chosen for the same gliders, the collision results are possibly not coincident with the above results. For convenience, we only select a fixed glider factor for each glider, and it has no effect on the observations of complex collisions concerning two gliders in this subsection. The abbreviations of the glider factors are provided in Table 2.

Specially, glider factors are captured as $NE \cup [\xi] \cup NE$, the natural number N represents the number of ether factor. Subsequently, the collision results depend on a periodic manner according to the different number of ether factors between two gliders. Let Q denote the value of this period. Each collision formula is introduced as

$$[\xi] \cup (QN + I)E \cup [\eta] \to \{\text{results}\},$$

where $QN + I$ is the number of ether factor E between two gliders, N is a natural number and $I = 1, 2, \ldots, Q$. However, if the two gliders have

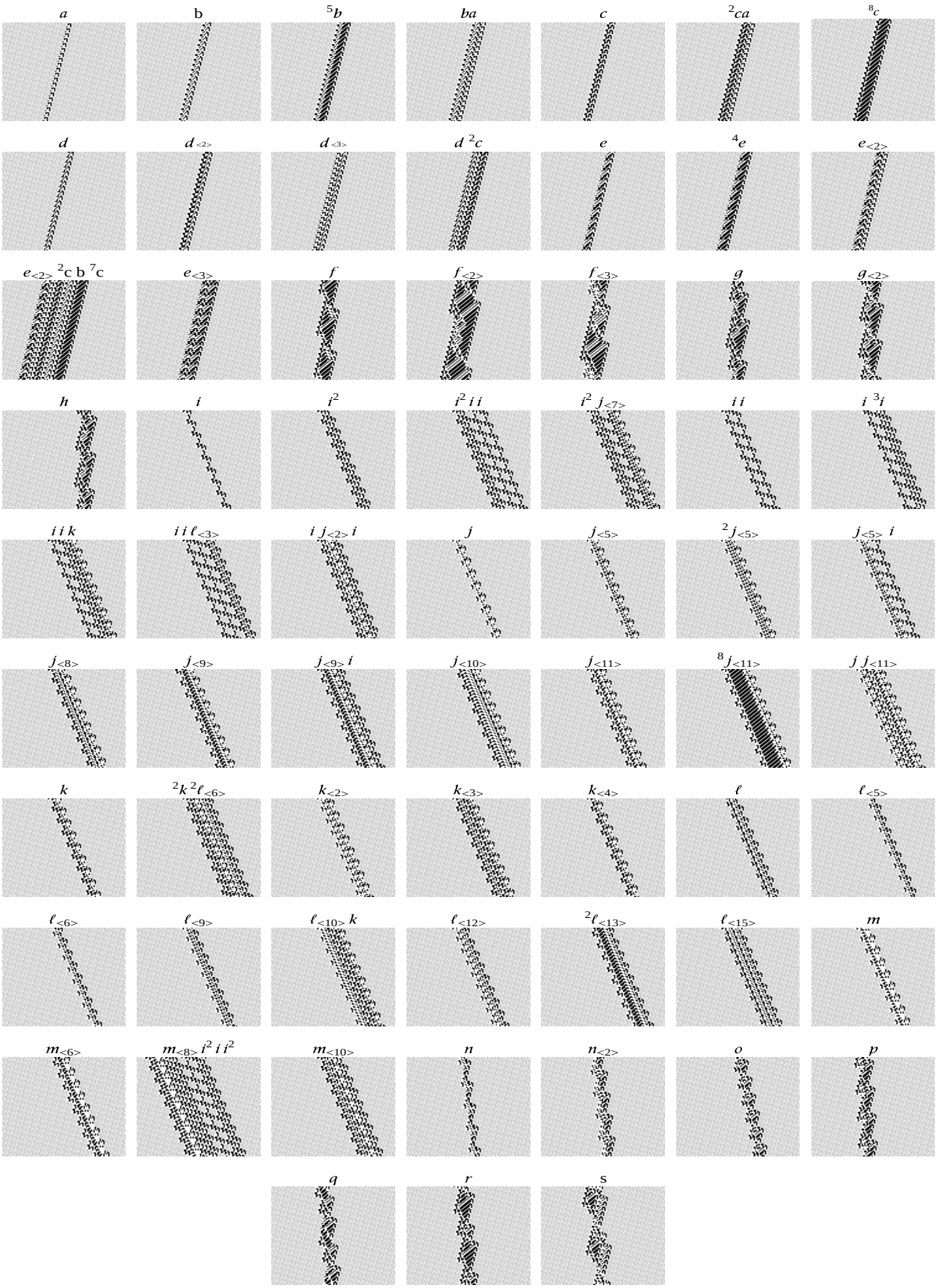

Fig. 8. The spatiotemporal patterns of several gliders.

Table 1. Characterizations of OGs and DCGs.

Glider	Velocity	With	Glider	Velocity	With
Ether unit	−1/5	1–6			
a	−1/5	3–4	${}^{2}j_{\langle 5\rangle}$	4/12	8–14
b	−1/5	7–8	$j_{\langle 5\rangle}\ i$	4/12	15–21
${}^{5}b$	−1/5	11–12	$j_{\langle 8\rangle}$	4/12	11–17
ba	−1/5	11–12	$j_{\langle 9\rangle}$	4/12	11–17
c	−1/5	7–8	$j_{\langle 9\rangle}\ i$	4/12	19–25
${}^{2}c\ a$	−1/5	11–12	$j_{\langle 10\rangle}\ i$	4/12	19
${}^{8}c$	−1/5	12–13	$j_{\langle 11\rangle}$	4/12	12–18
d	−1/5	5–6	${}^{8}j_{\langle 11\rangle}$	4/12	20–26
$d_{\langle 2\rangle}$	−1/5	8–9	$j\ j_{\langle 11\rangle}$	4/12	20–24
$d_{\langle 3\rangle}$	−1/5	9–10	k	4/12	7–13
$d\ {}^{2}c$	−1/5	13–14	${}^{2}k\ {}^{2}l_{\langle 6\rangle}$	4/12	21–27
e	−2/10	7	$k_{\langle 2\rangle}$	4/12	10–14
${}^{4}e$	−2/10	9–10	$k_{\langle 3\rangle}$	4/12	14–20
$e_{\langle 2\rangle}$	−2/10	10	$k_{\langle 4\rangle}$	4/12	7–11
$e_{\langle 2\rangle}\ {}^{2}c\ b\ {}^{7}c$	−2/10	37–38	l	4/12	9–15
$e_{\langle 3\rangle}$	−2/10	14	$l_{\langle 5\rangle}$	4/12	5–11
f	−2/42	9–16	$l_{\langle 6\rangle}$	4/12	5–9
$f_{\langle 2\rangle}$	−7/68	19–26	$l_{\langle 9\rangle}$	4/12	10
$f_{\langle 3\rangle}$	−4/84	9–23	$l_{\langle 10\rangle}\ k$	4/12	19–23
g	−1/69	10–17	$l_{\langle 12\rangle}$	4/12	10–16
$g_{\langle 2\rangle}$	−1/37	12–19	${}^{2}l_{\langle 13\rangle}$	4/12	13–19
h	−1/37	10–14	$l_{\langle 15\rangle}$	4/12	13–19
i	4/12	3–9	m	4/12	7–13
i^2	4/12	7–13	$m_{\langle 6\rangle}$	4/12	11–15
$i^2\ ii$	4/12	25–30	$m_{\langle 8\rangle}\ i^2\ i\ i^2$	4/12	45–51
$i^2\ j_{\langle 7\rangle}$	4/12	23–29	$m_{\langle 10\rangle}$	4/12	17–23
ii	4/12	12–16	n	2/22	4–11
$i\ {}^{3}i$	4/12	16–19	$n_{\langle 2\rangle}$	2/22	9–15
iik	4/12	20–26	o	3/17	6–12
$ii\ l_{\langle 3\rangle}$	4/12	23–29	p	1/27	10–17
$i\ j_{\langle 2\rangle}i$	4/12	15–19	q	3/49	6–17
j	4/12	3–9	r	3/49	8–15
$j_{\langle 5\rangle}$	4/12	6–12	s	3/49	8–21

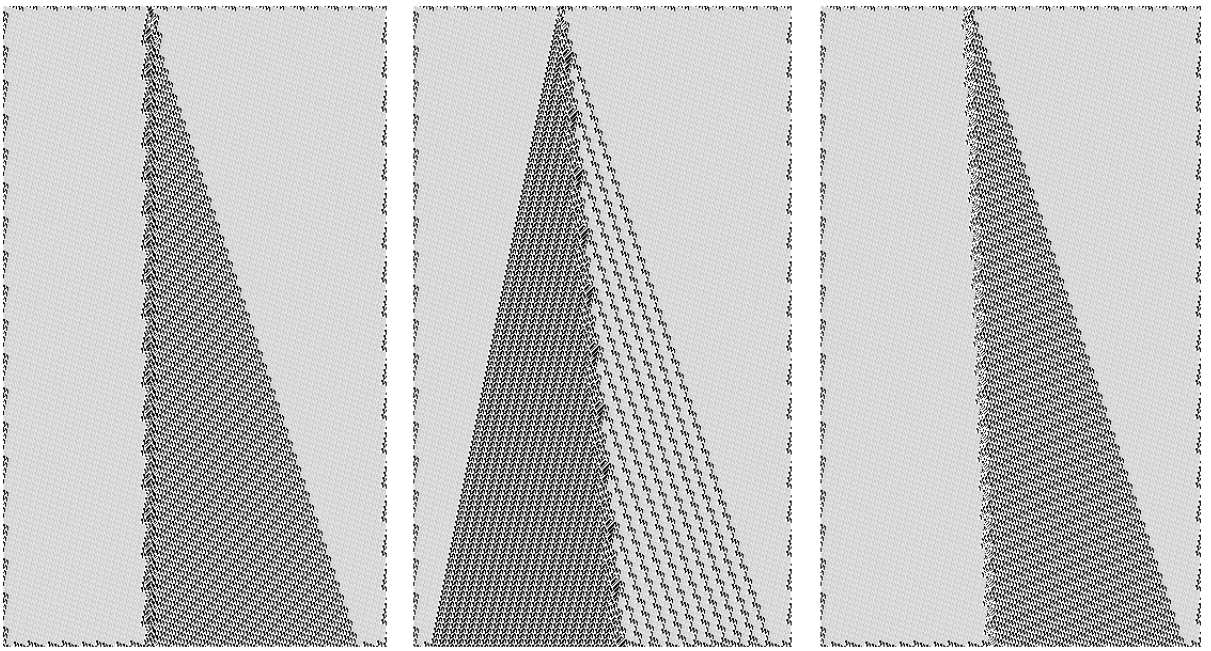

Fig. 9. The spatiotemporal patterns of three fusions.

Table 2. Decimal expressions of glider factors.

Glider Factor	With	Decimal Expression
$[a]$	23	(6889542/5839766/4741812)
$[b]$	14	(12870/10262/9652)
$[^5b]$	18	(242246/186390/189876)
$[ba]$	37	(112883053126/95677458454/77690201524)
$[c]$	20	(863814/729622/592308)
$[^2c\ a]$	31	(1763724870/1494979094/1213905332)
$[^8c]$	32	(3527601734/2989978134/2427828660)
$[d]$	12	(3526/2582/2356)
$[d_{\langle 2\rangle}]$	28	(220474950/186871318/151736756)
$[d_{\langle 3\rangle}]$	35	(28220760134/23919367062/19422546612)
$[d\ ^2c]$	20	(945606/748054/739636)
$[e]$	39	(451532235334/382709860630/310760758452)
$[^4e]$	35	(28220764742/23910988054/19422551220)
$[e_{\langle 2\rangle}]$	42	(3612257891910/3061678871446/2486086067636)
$[e_{\langle 2\rangle}\ ^2c\ b\ ^7c]$	44	(16384381235782/12604123124118/12870253732020)
$[e_{\langle 3\rangle}]$	46	(57796126291526/48986862228374/39777377117620)
$[f]$	35	(28220765894/23919376918/19422551220)
$[f_{\langle 2\rangle}]$	32	(3538817606/2994143766/2428182964)
$[f_{\langle 3\rangle}]$	16	(58054/46102/45236)
$[g]$	42	(3612257891910/3061678885270/2486086067636)
$[g_{\langle 2\rangle}]$	25	(27641926/23389206/18969012)
$[h]$	26	(55117382/46713238/37936564)

(*Continued*)

Table 2. (*Continued*)

Glider Factor	With	Decimal Expression
$[i]$	16	(53830/45590/37044)
$[i^2]$	32	(3527594566/2989920790/2427818164)
$[i^2\ ii]$	32	(3594703430/2987823638/2444595380)
$[i^2\ j_{\langle 7\rangle}]$	36	(56417768006/47793476118/38691770548)
$[ii]$	32	(3527594566/2989928982/2427818164)
$[i\ {}^3i]$	32	(3527857734/2989928982/2444530100)
$[iik]$	39	(451512816198/382691881494/310759493812)
$[ii\ l_{\langle 3\rangle}]$	29	(407032390/372683286/364220596)
$[i\ j_{\langle 2\rangle}\ i]$	31	(1763918406/1494962710/1213862068)
$[j]$	15	(26694/22678/18484)
$[j_{\langle 5\rangle}]$	12	(2246/2710/564)
$[{}^2j_{\langle 5\rangle}]$	33	(7055190726/5979834518/4855633460)
$[j_{\langle 5\rangle}\ i]$	28	(220489926/186739350/151732788)
$[j_{\langle 8\rangle}]$	23	(6834246/5804566/4732340)
$[j_{\langle 9\rangle}]$	42	(2228320654918/2846258270742/801291735476)
$[j_{\langle 9\rangle}\ i]$	26	(56133190/46667286/38123700)
$[j_{\langle 10\rangle}\ i]$	51	(1849476033873478/1567579581981206/1272876053918132)
$[j_{\langle 11\rangle}]$	25	(27543110/23332374/18892852)
$[{}^8j_{\langle 11\rangle}]$	45	(28898059284038/24493403108886/19888669964340)
$[jj_{\langle 11\rangle}]$	40	(903059040326/765425440790/621519128628)
$[k]$	39	(451532234822/382709858838/310760755636)
$[{}^2k\ {}^2l_{\langle 6\rangle}]$	28	(224990790/186712598/151523508)
$[k_{\langle 2\rangle}]$	30	(881893958/747485718/606952116)
$[k_{\langle 3\rangle}]$	20	(579654/710166/177588)
$[k_{\langle 4\rangle}]$	23	(6889542/5838358/4739508)
$[l]$	16	(49734/45590/42164)
$[l_{\langle 5\rangle}]$	37	(112883062342/95677485590/77690180020)
$[l_{\langle 6\rangle}]$	21	(1722438/1458710/1184948)
$[l_{\langle 9\rangle}]$	42	(3612257884870/3061678889110/2486086063668)
$[l_{\langle 10\rangle}\ k]$	39	(451529856710/382712853526/310759428276)
$[l_{\langle 12\rangle}]$	36	(56441530950/47838732822/38845090484)
$[{}^2l_{\langle 13\rangle}]$	44	(14449031801414/12246715560470/9944343228724)
$[l_{\langle 15\rangle}]$	32	(3527578182/2989896854/2427826612)
$[m]$	32	(3527595462/2989916182/2427814196)
$[m_{\langle 6\rangle}]$	27	(110193222/93401622/75510196)
$[m_{\langle 8\rangle}\ i^2\ i\ i^2]$	64	(15150907678911532102/12841647197503522326/10427119246272452020)
$[m_{\langle 10\rangle}]$	23	(6834246/4768278/4756916)
$[n]$	24	(13779526/11679254/9483828)
$[n_{\langle 2\rangle}]$	41	(1806128941254/1530839442582/1243043033652)
$[o]$	31	(1763797574/1494960150/1213909428)
$[p]$	23	(6911558/5846038/4742580)
$[q]$	18	(215110/182678/147892)
$[r]$	15	(30406/23062/23732)
$[s]$	15	(1726534/1459606/1184180)

only one collision result, the collision formula is simplified into $[\xi] \cup [\eta] \rightarrow \{\text{results}\}$, for instance, $[i] \cup [b] \rightarrow \{j\}$.

4. A Symbolic Dynamics Perspective of the Gliders in HCAM

4.1. *The fundamental concepts of symbolic dynamics*

In order to introduce a symbolic vector map F in the following, the original symbolic space S^Z must be extended to symbolic vector space

$$S_n^Z = \{X = ({x^{(1)}}^T, {x^{(2)}}^T, \ldots, {x^{(n)}}^T)^T \mid {x^{(j)}}^T \in S^Z, j = 1, 2, \ldots, n\},$$

where T refers to the transposed operation. Thus, the metric d^* on S_n^Z is defined as

$$d^*(X, \overline{X}) = \left(\sum_{j=1}^{n} d(x^{(j)}, \overline{x}^{(j)}) \right)^{\frac{1}{n}}.$$

Obviously, d^* satisfies the distance conditions of non-negativity, symmetry and transitivity. Consequently, the definition of symbolic vector map $F : S_n^Z \rightarrow S_n^Z$ is

$$F \begin{pmatrix} x^{(1)} \\ x^{(2)} \\ \vdots \\ x^{(n)} \end{pmatrix} = \begin{pmatrix} f(x^{(1)}) \\ f(x^{(2)}) \\ \vdots \\ f(x^{(n)}) \end{pmatrix},$$

where $f : S^Z \rightarrow S^Z$ is the symbolic sequence map [Chen *et al.*, 2012; Zhou, 1997]. (S_n^Z, F) is a compact dynamical system.

Definition 4.1. F is chaotic on S_n^Z in the sense of Li–Yorke if

(1) $\lim\limits_{n\rightarrow\infty} \sup d(F^n(X), F^n(Y)) > 0,$

$$\forall\, X, Y \in S_n^Z,\ \ X \neq Y;$$

(2) $\lim\limits_{n\rightarrow\infty} \inf d(F^n(X), F^n(Y)) = 0, \quad \forall\, X, Y \in S_n^Z.$

We say $X \in S_n^Z$ is a n-periodic point of F if there exists the integer $n > 0$ such that $F^n(X) = X$. Let $P(F)$ stand for the set of all n-period points, that is, $P(F) = \{X \in S_n^Z \mid \exists\, n > 0, F^n(X) = X\}$. In particular, if $F(X) = X$ for several $X \in S_n^Z$, X is fixed point. Then, F is said to be topologically transitive if for any nonempty open subsets U and V of S_n^Z there exists a natural number n such that $F^n(U) \cap V \neq \emptyset$. $P(F)$ is called a dense subset of S_n^Z if, for any $X \in S_n^Z$ and any constant $\varepsilon > 0$, there exists a $Y \in P(F)$ such that $d(x, y) < \varepsilon$. F is sensitive to initial conditions if there exists a $\delta > 0$ such that, for $X \in S_n^Z$ and for any neighborhood $B(X)$ of X, there exists a $Y \in B(X)$ and a natural number n such that $d(F^n(X), F^n(Y)) > \delta$.

Definition 4.2. F is chaotic on S_n^Z in the sense of Devaney if (1) F is transitive; (2) $P(F)$ is a dense subset of S_n^Z; (3) F is sensitive to initial conditions.

Let $R \subset S_n^Z$ be called a (n, ε)-spanning set iff for any $X \in S_n^Z$ and any constant $n > 0$, $\varepsilon > 0$, there exists a $Y \in R$ such that $d(F^i(X), F^i(Y)) \leq \varepsilon$, $i = 0, 1, \ldots, n-1$. Thus, $r_n(\varepsilon, S_n^Z, F)$ stands for the infimum of cardinal number of (n, ε)-spanning set with F. The Bowen's topological entropy is defined as follows:

$$\text{ent}(F) = \lim_{\varepsilon\rightarrow\infty} \lim_{n\rightarrow\infty} \sup \frac{1}{n} \log r_n(\varepsilon, S_n^Z, F).$$

In addition, F is topologically mixing if there exists a natural number N such that $F^n(U) \cap V \neq \emptyset$ for the entire $n \geq N$.

Theorem 1

(1) *F is chaos in the sense of Li–Yorke and this can be deduced from positive topological entropy.*
(2) *F is chaos in the sense of Devaney and Li–Yorke and this can be deduced from topologically mixing.*

A set $X \subseteq S_n^Z$ is F-invariant if $F(X) \subseteq X$ and strongly F-invariant if $F(X) = X$. If X is closed and F-invariant, then (X, F) or simply X is called a subsystem of F. A set $X \subseteq S_n^Z$ is an attractor if there exists a nonempty clopen F-invariant set Y such that

$$\bigcap_{t\geq 0} F^t(Y) = X.$$

For instance, fixed point set and periodic point set are two types of simple attractor. Furthermore, there always exists a global attractor, denoted by

$$\Lambda = \bigcap_{t\geq 0} F^t(S_n^Z),$$

which is also called the limit set of F.

As every column of X is $X_i = (x_i^{(1)}, x_i^{(2)}, \ldots, x_i^{(n)})^T$, the right shift map σ is defined by $[\sigma(X)]_i = X_{i-1}$ for any $X \in S_n^Z$, $i \in Z$. We call the $n \times i$-word block as

$$\begin{pmatrix} a_1^{(1)} & \cdots & a_i^{(1)} \\ & \cdots & \\ a_1^{(n)} & \cdots & a_i^{(n)} \end{pmatrix}$$

of elements of S_n^Z. Let $\mathcal{A}$ denote a set of some finite $n \times i$-word blocks over S_n^Z, and $\Lambda = \Lambda_{\mathcal{A}}$ is the set which consists of the bi-infinite configurations made up of all the word blocks in $\mathcal{A}$. Then, $\Lambda_{\mathcal{A}}$ is a subsystem of (S_n^Z, σ), where $\mathcal{A}$ is said to be the determinative system of Λ. For a closed invariant subset $\Lambda \subseteq S_n^Z$, the subsystem (Λ, σ) or simply Λ is called a subshift of σ.

In order to find the subsystem of finite type, it is important to assume that the initial configurations of original stipulation shall be applicable, *mutatis mutandis*, to the mathematical definition of ECAM rules. When $t < 3$, the first three lines of cell array of HCAM$(43, 74)$ are all regarded as the random initial configurations; that is, the second and third lines of cell array are not regarded to be the evolution results of the first line according to the ECA rules. When $t \geq 3$, it evolves following the original approach. Consequently, the new evolution rule F will be conformed to the mathematical definition of the function.

At the moment, let $n = 3$, then $S_n^Z = S_3^Z$. The symbolic vector map $F : S_3^Z \to S_3^Z$ is expressed as

$$F\begin{pmatrix} x^{(1)} \\ x^{(2)} \\ x^{(3)} \end{pmatrix} = \begin{pmatrix} x^{(2)} \\ x^{(3)} \\ f_{74} \circ f_{43}({x^{(1)}}^T, {x^{(2)}}^T, {x^{(3)}}^T)^T \end{pmatrix} = \begin{pmatrix} x^{(2)} \\ x^{(3)} \\ x^{(4)} \end{pmatrix}.$$

Analogously,

$$F^2\begin{pmatrix} x^{(1)} \\ x^{(2)} \\ x^{(3)} \end{pmatrix} = \begin{pmatrix} x^{(3)} \\ x^{(4)} \\ f_{74} \circ f_{43}({x^{(2)}}^T, {x^{(3)}}^T, {x^{(4)}}^T)^T \end{pmatrix} = \begin{pmatrix} x^{(3)} \\ x^{(4)} \\ x^{(5)} \end{pmatrix}.$$

Based on the above analysis, the functional form of F^t is defined as

$$F^t\begin{pmatrix} x^{(1)} \\ x^{(2)} \\ x^{(3)} \end{pmatrix} = \begin{pmatrix} f_{74} \circ f_{43}({x^{(t-2)}}^T, {x^{(t-1)}}^T, {x^{(t)}}^T)^T \\ f_{74} \circ f_{43}({x^{(t-1)}}^T, {x^{(t)}}^T, {x^{(t+1)}}^T)^T \\ f_{74} \circ f_{43}({x^{(t)}}^T, {x^{(t+1)}}^T, {x^{(t+2)}}^T)^T \end{pmatrix},$$

where $t \in N$ and $t \geq 3$.

4.2. *Complex shift dynamics of gliders*

In the following, an analytical method on the discussion of the symbolic dynamics of the gliders in HCAM$(43, 74)$ is carried out. For each glider, a particular subsystem of (S_3^Z, F) can be found through enumeration and computer programming. Then, the key question is whether the evolution function is topologically mixing and possesses the positive topological entropy on this subsystem. For clarity and convenience, only the glider e is described in detail.

Proposition 1. *For glider e, there exists a subset $\Lambda_{\mathcal{A}}$ of S_3^Z, such that*

$$F^{10}(X)|_{\Lambda_{\mathcal{A}}} = \sigma_L(X)|_{\Lambda_{\mathcal{A}}}, \quad \forall\, X \in \Lambda_{\mathcal{A}},$$

where

$$\Lambda_{\mathcal{A}} = \left\{ X = \begin{pmatrix} x^{(1)} \\ x^{(2)} \\ x^{(3)} \end{pmatrix} \in S_3^Z, \forall\, i \in Z, \begin{pmatrix} x_i^{(1)} & x_{i+1}^{(1)} & \cdots & x_{i+18}^{(1)} & x_{i+19}^{(1)} \\ x_i^{(2)} & x_{i+1}^{(2)} & \cdots & x_{i+18}^{(2)} & x_{i+19}^{(2)} \\ x_i^{(3)} & x_{i+1}^{(3)} & \cdots & x_{i+18}^{(3)} & x_{i+19}^{(3)} \end{pmatrix} \in \mathcal{A} \right\},$$

where

$$\begin{aligned}\mathcal{A} = \{&(185926/430614/364980), (92963/739595/706778), (46481/894085/877677),\\ &(547528/447042/438838), (273764/223521/743707), (136882/111760/371853),\\ &(592729/580168/185926), (296364/290084/92963), (148182/145042/46481),\\ &(598379/596809/547528), (299189/822692/273764), (673882/411346/136882),\\ &(861229/729961/592729), (430614/364980/296364), (739595/706778/148182),\\ &(894085/877677/598379), (447042/438838/299189), (223521/743707/673882),\\ &(111760/371853/861229), (580168/185926/430614), (290084/92963/739595),\\ &(145042/46481/894085), (596809/547528/447042), (822692/273764/223521),\\ &(411346/136882/111760), (729961/592729/580168), (364980/296364/290084),\\ &(706778/148182/145042), (877677/598379/596809), (438838/299189/822692),\\ &(743707/673882/411346), (371853/861229/729961), (145042/570769/369797),\\ &(596809/285384/184898), (298404/142692/616737), (149202/595634/832656),\\ &(74601/297817/940616), (561588/148908/470308), (280794/74454/759442),\\ &(140397/37227/904009), (594486/542901/452004), (821531/271450/226002),\\ &(410765/135725/113001), (729670/592150/580788), (364835/296075/290394),\\ &(706705/148037/145197), (877640/598306/596886), (438820/299153/822731),\\ &(743698/673864/411365), (371849/861220/729970), (185924/430610/364985),\\ &(92962/739593/706780), (46481/894084/877678), (547528/447042/438839),\\ &(92963/739595/182490), (570769/369797/91245), (285384/184898/569910),\\ &(142692/616737/809243), (595634/832656/404621), (297817/940616/726598),\\ &(148908/470308/363299), (74454/759442/705937), (37227/904009/877256),\\ &(542901/452004/438628), (271450/226002/743602), (135725/113001/371801),\\ &(592150/580788/185900), (296075/290394/92950), (148037/145197/46475),\\ &(598306/596886/547525), (299153/822731/273762), (673864/411365/136881),\\ &(861220/729970/592728), (430610/364985/296364), (739593/706780/148182),\\ &(894084/877678/598379), (447042/438839/299189), (430614/364980/820652),\\ &(739595/182490/410326), (369797/91245/729451), (184898/569910/889013),\\ &(616737/809243/968794), (832656/404621/484397), (940616/726598/766486),\\ &(470308/363299/383243), (759442/705937/191621), (904009/877256/620098),\\ &(452004/438628/310049), (226002/743602/679312), (113001/371801/863944),\\ &(580788/185900/431972), (290394/92950/740274), (145197/46475/894425),\\ &(596886/547525/447212), (822731/273762/223606), (411365/136881/111803),\\ &(729970/592728/580189), (364985/296364/290094), (706780/148182/145047),\end{aligned}$$

(877678/598379/596811), (438839/299189/822693), (364980/820652/290084), (182490/410326/145042), (91245/729451/596809), (569910/889013/822692), (809243/968794/411346), (404621/484397/205673), (726598/766486/627124), (363299/383243/313562), (705937/191621/156781), (877256/620098/602678), (438628/310049/825627), (743602/679312/412813), (371801/863944/730694), (185900/431972/365347), (92950/740274/706961), (46475/894425/877768), (547525/447212/438884), (273762/223606/743730), (136881/111803/371865), (592728/580189/185932), (296364/290094/92966), (148182/145047/46483), (598379/596811/547529), (299189/822693/273764), (820652/290084/617251), (410326/145042/832913), (729451/596809/940744), (889013/822692/470372), (968794/411346/759474), (484397/205673/379737), (766486/627124/189868), (383243/313562/94934), (191621/156781/47467), (620098/602678/548021), (310049/825627/274010), (679312/412813/137005), (863944/730694/592790), (431972/365347/296395), (740274/706961/148197), (894425/877768/598386), (447212/438884/299193), (223606/743730/673884), (111803/371865/861230), (580189/185932/430615), (290094/92966/739595), (145047/46483/894085), (596811/547529/447042), (822693/273764/223521), (290084/617251/739595), (145042/832913/894085), (596809/940744/447042), (822692/470372/747809), (411346/759474/898192), (205673/379737/973384), (627124/189868/486692), (313562/94934/767634), (156781/47467/908105), (602678/548021/454052), (825627/274010/227026), (412813/137005/113513), (730694/592790/581044), (365347/296395/290522), (706961/148197/145261), (877768/598386/596918), (438884/299193/822747), (743730/673884/411373), (371865/861230/729974), (185932/430615/364987), (92966/739595/706781), (46483/894085/877678), (547529/447042/438839), (617251/739595/706778), (832913/894085/877677), (940744/447042/438838), (470372/747809/743707), (759474/898192/371853), (379737/973384/710214), (189868/486692/355107), (94934/767634/701841), (47467/908105/875208), (548021/454052/437604), (274010/227026/743090), (137005/113513/371545), (592790/581044/185772), (296395/290522/92886), (148197/145261/46443), (598386/596918/547509), (299193/822747/273754), (673884/411373/136877), (861230/729974/592726), (430615/364987/296363), (739595/706781/148181), (894085/877678/598378), (739595/706778/410326), (894085/877677/205163), (447042/438838/626869), (747809/743707/313434), (898192/371853/156717), (973384/710214/602646), (486692/355107/301323),

(767634/701841/150661), (908105/875208/599618), (454052/437604/299809),
(227026/743090/674192), (113513/371545/861384), (581044/185772/430692),
(290522/92886/739634), (145261/46443/894105), (596918/547509/447052),
(822747/273754/223526), (411373/136877/111763), (729974/592726/580169),
(364987/296363/290084), (706781/148181/145042), (877678/598378/596809),
(438839/299189/822692), (706778/410326/145042), (877677/205163/596809),
(438838/626869/298404), (743707/313434/149202), (371853/156717/74601),
(710214/602646/561588), (355107/301323/280794), (701841/150661/140397),
(875208/599618/594486), (437604/299809/821531), (743090/674192/410765),
(371545/861384/729670), (185772/430692/364835), (92886/739634/706705),
(46443/894105/877640), (547509/447052/438820), (273754/223526/743698),
(136877/111763/371849), (592726/580169/185924), (296363/290084/92962),
(148181/145042/46481), (598378/596809/547528), (820652/290084/92963),
(410326/145042/570769), (205163/596809/285384), (626869/298404/142692),
(313434/149202/595634), (156717/74601/297817), (602646/561588/148908),
(301323/280794/74454), (150661/140397/37227), (599618/594486/542901),
(299809/821531/271450), (674192/410765/135725), (861384/729670/592150),
(430692/364835/296075), (739634/706705/148037), (894105/877640/598306),
(447052/438820/299153), (223526/743698/673864), (111763/371849/861220),
(580169/185924/430610), (290084/92962/739593), (145042/46481/894084)}.

Remark 4.1. The $\mathcal{A}$ is the determinative system of $\Lambda_{\mathcal{A}}$, which is a 3×19-word blocks set. For convenience, each element in $\mathcal{A}$ is described by its decimal code expression, such as (185926/430614/364980) that refers to the 3×19-word block

$$\begin{pmatrix} 0,1,1,0,0,0,1,0,0,1,1,0,1,0,1,1,0,1,0,0 \\ 0,1,1,0,1,0,0,0,0,1,0,0,1,0,0,1,0,1,1,0 \\ 0,0,1,0,1,1,0,1,1,0,0,0,1,0,0,1,1,0,1,0 \end{pmatrix},$$

where the integers are respectively decimal code expressions of three lines string.

In a nutshell, directed graph theory provides a powerful tool for studying the infinite configurations. A fundamental method for constructing finite shifts starts with a finite, directed graph and produces the collection of all bi-infinite walks (i.e. strings of edges) on the graph. A graph $G(V, E)$ consists of a finite set V of vertices (or states) together with a finite set E of edges. $\Lambda_{\mathcal{A}}$ can be described by a finite directed graph $G_{\mathcal{A}}$, where each vertex is a 3×20-block in $\mathcal{A}$. Each edge $e \in E$ starts at a block denoted by $(X_{3\times 20}) \in \mathcal{A}$ and terminates at the string $(X'_{3\times 20}) \in \mathcal{A}$ if and only if

$$\begin{pmatrix} x_{i+1}^{(1)} & \cdots & x_{i+18}^{(1)} & x_{i+19}^{(1)} \\ x_{i+1}^{(2)} & \cdots & x_{i+18}^{(2)} & x_{i+19}^{(2)} \\ x_{i+1}^{(3)} & \cdots & x_{i+18}^{(3)} & x_{i+19}^{(3)} \end{pmatrix} = \begin{pmatrix} x_{i}^{(1)'} & x_{i+1}^{(1)'} & \cdots & x_{i+18}^{(1)'} \\ x_{i}^{(2)'} & x_{i+1}^{(2)'} & \cdots & x_{i+18}^{(2)'} \\ x_{i}^{(3)'} & x_{i+1}^{(3)'} & \cdots & x_{i+18}^{(3)'} \end{pmatrix}.$$

One can represent each element of $\Lambda_{\mathcal{A}}$ as a certain path on the graph $G_{\mathcal{A}}$. The entire bi-infinite walks on the graph constitute the closed invariant subsystem $\Lambda_{\mathcal{A}}$. The finite directed graph $\Lambda_{\mathcal{A}}$, is shown in Fig. 10.

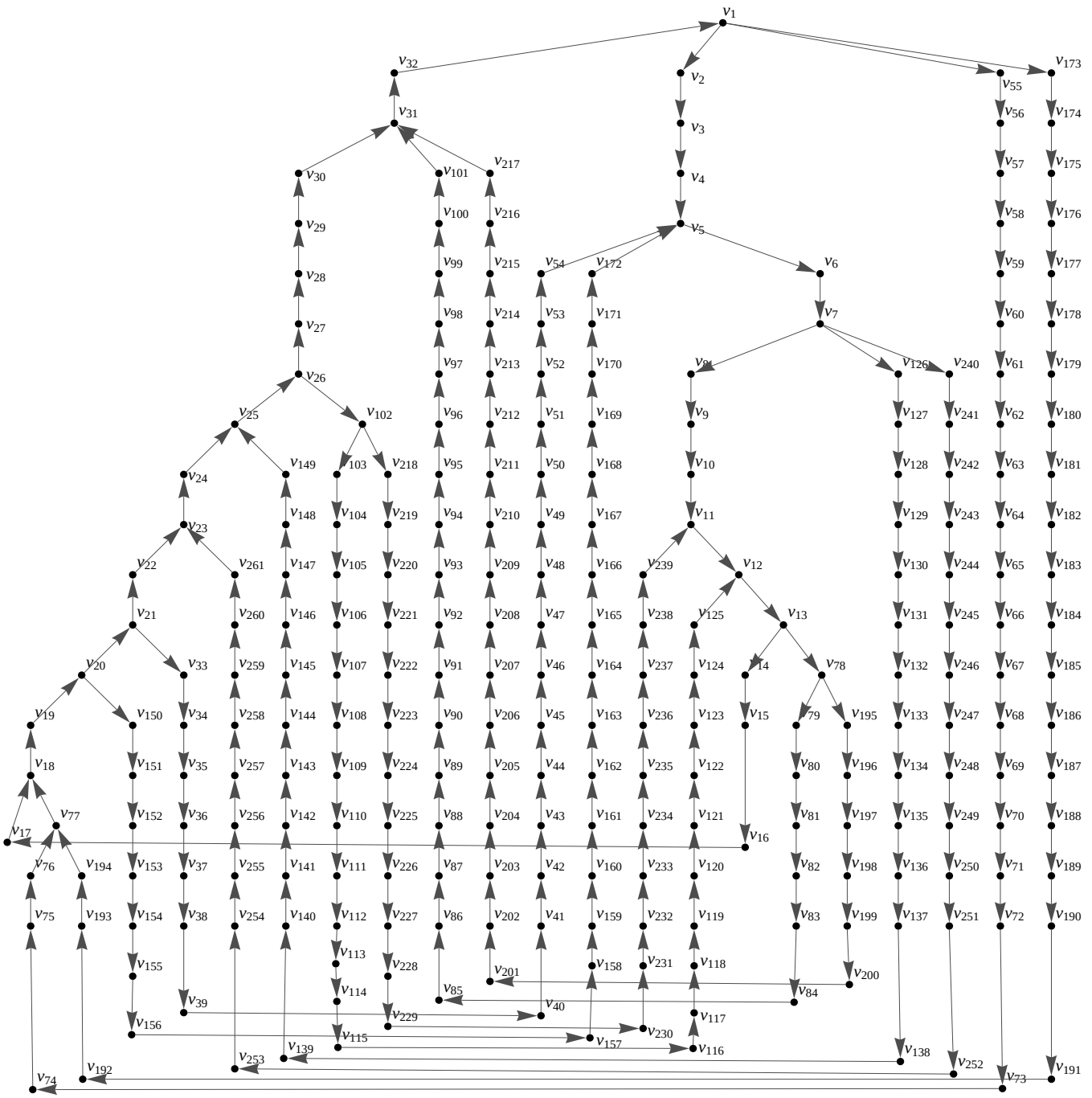

Fig. 10. Graph representation for the subsystem $\Lambda_{\mathcal{A}}$ of glider e.

It can be extrapolated accurately that the finite directed graph $G_{\mathcal{A}}$ only consists of the different cycles. A cycle is a path that starts and terminates at the same vertex. When one cycle has repeated vertices, it is called the reducible cycle; otherwise, it is called the irreducible cycle. Any cycle can be compounded by the irreducible cycle. And the period with period points of F on $\Lambda_{\mathcal{A}}$ is the length of the cycle. The irreducible cycle can produce the irreducible period point of F. As the length of irreducible cycle is less than the number of vertices, F has finite different periods. It is of interest that the irreducible cycles actually define a series of minimal sets M of $\Lambda_{\mathcal{A}}$. The minimal sets imply the smallest subsystems of $\Lambda_{\mathcal{A}}$, which are endowed with simple dynamical properties. Then, $F^{10}|_M$ is topologically transitive, yet has zero topological entropy.

Let $\hat{S} = \{r_0, r_1, \ldots, r_{259}, r_{260}\}$ be a new symbolic set, where r_i, $i = 0, \ldots, 260$, stand for elements of $\mathcal{A}$ respectively. Then, $r_i = (b_0^i b_1^i \cdots b_{18}^i b_{19}^i)$ are 3×20 matrix and corresponding column vectors of r_i are expressed as $b_0^i, b_1^i, \ldots, b_{19}^i$, which only contain eight different statuses, such as $(0,0,0)^T$, $(0,0,1)^T$, $(0,1,0)^T$, $(0,1,1)^T$, $(1,0,0)^T$, $(1,0,1)^T$, $(1,1,0)^T$, $(1,1,1)^T$. Then, one can construct a new symbolic space $\hat{S}^Z$ on $\hat{S}$. Denote by $\mathcal{B} = \{(r_i r_j) \,|\, r_i = (b_0^i b_1^i \cdots b_{18}^i b_{19}^i),\ r_j = (b_0^j b_1^j \cdots b_{18}^j b_{19}^j) \in \hat{S},\ \forall 1 \le p \le 19 \text{ s.t. } b_p^i = b_{p-1}^j\}$. Furthermore, the two-order subshift $\Lambda_{\mathcal{B}}$ of σ_L is defined by $\Lambda_{\mathcal{B}} = \{r = (\cdots, r_{-1}, r_0^*, r_1, \cdots) \in \hat{S}^Z \,|\, r_i \in \hat{S}, (r_i, r_{i+1}) \prec \mathcal{B}, \forall\, i \in Z\}$. Therefore, it is easy to calculate the transition matrix $\mathcal{D}$ of the subshift $\Lambda_{\mathcal{B}}$. The matrix $\mathcal{D}$ is positive if all of its entries are non-negative, irreducible if $\forall\, t, i$, there exist n such that $\mathcal{D}_{ti}^n > 0$, and aperiodic if there exists N, such that $D_{ti}^n > 0$, $n > N$, $\forall\, t, i$. $\Lambda_{\mathcal{B}}$ is topologically mixing if and only if $\mathcal{D}$ is irreducible and aperiodic. In addition, the transition matrix $\mathcal{D}$ is relatively large (the order of D is 261). Therefore, we only list the indices (i, j) of nonzero elements.

$\mathcal{D} = \{(1,2),(1,55),(1,173),(2,3),(3,4),(4,5),(5,6),(6,7),(7,8),(7,126),(7,240),(8,9),(9,10),(10,11),$
$(11,12),(12,13),(13,14),(13,78),(14,15),(15,16),(16,17),(17,18),(18,19),(19,20),(20,21),$
$(20,150),(21,22),(21,33),(22,23),(23,24),(24,25),(25,26),(26,27),(26,102),(27,28),(28,29),$
$(29,30),(30,31),(31,32),(32,1),(33,34),(34,35),(35,36),(36,37),(37,38),(38,39),(39,40),(40,41),$
$(41,42),(42,43),(43,44),(44,45),(45,46),(46,47),(47,48),(48,49),(49,50),(50,51),(51,52),(52,53),$
$(53,54),(54,55),(55,56),(56,57),(57,58),(58,59),(59,60),(60,61),(61,62),(62,63),(63,64),(64,65),$
$(65,66),(66,67),(67,68),(68,69),(69,70),(70,71),(71,72),(72,73),(73,74),(74,75),(75,76),(76,77),$
$(77,18),(78,79),(78,195),(79,80),(80,81),(81,82),(82,83),(83,84),(84,85),(85,86),(86,87),$
$(87,88),(88,89),(89,90),(90,91),(91,92),(92,93),(93,94),(94,95),(95,96),(96,97),(97,98),(98,99),$
$(99,100),(100,101),(101,31),(102,103),(102,218),(103,104),(104,105),(105,106),(106,107),$
$(107,108),(108,109),(109,110),(110,111),(111,112),(112,113),(113,114),(114,115),(115,116),$
$(116,117),(117,118),(118,119),(119,120),(120,121),(121,122),(122,123),(123,124),(124,125),$
$(125,12),(126,127),(127,128),(128,129),(129,130),(130,131),(131,132),(132,133),(133,134),$
$(134,135),(135,136),(136,137),(137,138),(138,139),(139,140),(140,141),(141,142),(142,143),$
$(143,144),(144,145),(145,146),(146,147),(147,148),(148,149),(149,25),(150,151),(151,152),$
$(152,153),(153,154),(154,155),(155,156),(156,157),(157,158),(158,159),(159,160),(160,161),$
$(161,162),(162,163),(163,164),(164,165),(165,166),(166,167),(167,168),(168,169),(169,170),$

$(170, 171), (171, 172), (172, 5), (173, 174), (174, 175), (175, 176), (176, 177), (177, 178), (178, 179),$
$(179, 180), (180, 181), (181, 182), (182, 183), (183, 184), (184, 185), (185, 186), (186, 187), (187, 188),$
$(188, 189), (189, 190), (190, 191), (191, 192), (192, 193), (193, 194), (194, 77), (195, 196), (196, 197),$
$(197, 198), (198, 199), (199, 200), (200, 201), (201, 202), (202, 203), (203, 204), (204, 205), (205, 206),$
$(206, 207), (207, 208), (208, 209), (209, 210), (210, 211), (211, 212), (212, 213), (213, 214), (214, 215),$
$(215, 216), (216, 217), (217, 31), (218, 219), (219, 220), (220, 221), (221, 222), (222, 223), (223, 224),$
$(224, 225), (225, 226), (226, 227), (227, 228), (228, 229), (229, 230), (230, 231), (231, 232), (232, 233),$
$(233, 234), (234, 235), (235, 236), (236, 237), (237, 238), (238, 239), (239, 11), (240, 241), (241, 242),$
$(242, 243), (243, 244), (244, 245), (245, 246), (246, 247), (247, 248), (248, 249), (249, 250), (250, 251),$
$(251, 252), (252, 253), (253, 254), (254, 255), (255, 256), (256, 257), (257, 258), (258, 259), (259, 260),$
$(260, 261), (261, 23)\}$.

Proposition 2. *The nonwandering set*

$$\Omega(F^{10}|_{\Lambda_{\mathcal{A}}}) = \Lambda_{\mathcal{A}}.$$

Proof. The elements of $\mathcal{D}^n$ are marked as $\mathcal{D}^n_{i,j}$, $1 \le i, j \le 261$. Here each $\mathcal{D}^n_{i,j}$ shows the number of all the paths from vertex v_i to vertex v_j whose length is n. Thus, $\mathcal{D}^n_{i,i}$ is the number of all cycles of ith vertex with length n. As $\mathcal{D}^n_{i,i}$ is positive for $n = 425$, it is easy to verify that each vertex has a particular cycle. ■

Proposition 3. *$F^{10}|_{\Lambda_{\mathcal{A}}}$ is topologically transitive.*

Proof. Here σ_L is topologically transitive on $\Lambda_{\mathcal{A}}$ if the transition matrix $\mathcal{D}$ is irreducible. Further, the irreducibility of $\mathcal{D}$ indicates that $\mathcal{D}+\mathcal{I}$ is aperiodic, where $\mathcal{I}$ is the 261×261 identity matrix. Meanwhile, it is easy to verify that $(\mathcal{D}+\mathcal{I})^n$ is positive for $n \ge 75$. Hence, F^{10} is topologically transitive on $\Lambda_{\mathcal{A}}$. ■

Proposition 4. *The topological entropy of $F^{10}|_{\Lambda_{\mathcal{A}}}$ is positive.*

Proof. Let $\rho(\mathcal{D})$ be the maximum positive real root λ^* of characteristic equation of $\mathcal{D}$. The characteristic equation is

$$-\lambda^{130}(\lambda^{131} - \lambda^{99} - 10\lambda^{92} - 40\lambda^{46} - 32) = 0.$$

The topological entropy of σ_L on $\Lambda_{\mathcal{A}}$ equals $\log \rho(\mathcal{D}) = 0.0667711$. ■

Proposition 5. *$F^{10}|_{\Lambda_{\mathcal{A}}}$ is topologically mixing.*

Proof. A two-order subshift of finite type is topologically mixing if and only if its transition matrix is irreducible and aperiodic. Meanwhile, it is easy to verify that $\mathcal{D}^n$ is positive for $n \ge 856$. This implies that $\mathcal{D}$ is irreducible and aperiodic. ■

Theorem 2. *$F^{10}|_{\Lambda_{\mathcal{A}}}$ is chaotic in the sense of both Li–Yorke and Devaney.*

Proof. The positive topological entropy implies chaos in the sense of Li–Yorke. Meanwhile, both the chaos in the sense of Devaney and in the sense of Li–Yorke can be deduced from topological mixing. ■

Remark 4.2. As a result, the dynamics of extant gliders can be analyzed and their dynamical characteristics are explored by the above method.

5. Concluding Remarks

Motivated by the cited works, HCAM rule is conceived when the memory function ($\tau = 3$) of ECAM rule is a concrete ECA rule. It is of interest in that a multitude of HCAM rules endowed with newfound and strong nonlinear spatiotemporal patterns are discovered by computer simulations and empirical observations. To cite a concrete case, HCAM$(43, 74)$ have a host of gliders and complicated glider collisions. After classifying and coding the gliders that frequently occurred in HCAM$(43, 74)$, we describe their collisions by introducing ether factor and glider factors.

Furthermore, through exploiting the mathematical definition of HCAM, we preliminarily explore an analytical method on the discussion of the symbolic dynamics of the gliders in HCAM(43, 74). Based on the directed graph representation and transition matrix, the evolution function of HCAM(43, 74) possesses the positive topological entropy and is topologically mixing on one subsystem of glider e. From the extant and newfound gliders, it is inferred that there exist many more chaotic subsystems. The method presented in this paper is also applicable to other HCAMs. In addition, the future work will be devoted to proving that HCAM(43, 74) is universal by simulating a cyclic tag system [Cook, 2004; Rendell, 2011, 2013].

References

Adamatzky, A. & Martínez, G. J. [2016] *Designing Beauty*: *The Art of Cellular Automata* (Springer, London).

Alonso-Sanz, R. & Martin, M. [2002] "One-dimensional cellular automata with memory: Patterns starting with a single site seed," *Int. J. Bifurcation and Chaos* **12**, 205–226.

Alonso-Sanz, R. & Martin, M. [2003] "Elementary cellular automata with memory," *Compl. Syst.* **14**, 99–126.

Alonso-Sanz, R. & Martin, M. [2004] "Three-state one-dimensional cellular automata with memory," *Chaos Solit. Fract.* **21**, 809–834.

Alonso-Sanz, R. & Martin, M. [2006] "Elementary cellular automata with elementary memory rules in cells: The case of linear rules," *J. Cell. Autom.* **1**, 70–86.

Alonso-Sanz, R. [2013] "Cellular automata with memory and the density classification task," *J. Cell. Autom.* **8**, 283–294.

Alonso-Sanz, R. [2016] "Cellular automata and other discrete dynamical systems with memory," *J. Cell. Autom.* **11**, 5–6.

Bingham, J. & Bingham, B. [2007] "Hybrid one-dimensional reversible cellular automata are regular," *Discr. Appl. Math.* **155**, 2555–2566.

Cattell, K. & Muzio, J. C. [1996] "Synthesis of one-dimensional linear hybrid cellular automata," *IEEE Trans. Comput.-Aided Design of Integr. Circuits Syst.* **15**, 325–335.

Chen, F. Y., Jin, W. F., Chen, G. R. & Chen, L. [2012] "Chaos emerged on the 'edge of chaos'," *Int. J. Comput. Math.* **89**, 1584–1595.

Chen, B., Chen, F. Y., Jin, W. F. & Guan, J. B. [2015] "A symbolic dynamics perspective of elementary cellular automaton rule 12 with minority memory," *J. Cell. Autom.* **10**, 393–408.

Chua, L. O., Pazienza, G. E. & Shin, J. [2005] "A nonlinear dynamics perspective of Wolfram's new kind of science. Part IV: From Bernoulli shift to $1/f$ spectrum," *Int. J. Bifurcation and Chaos* **15**, 1045–1183.

Chua, L. O., Pazienza, G. E., Orzo, L., Sbitnev, V. I. & Shin, J. [2008] "A nonlinear dynamics perspective of Wolfram's new kind of science. Part IX: Quasi-ergodicity," *Int. J. Bifurcation and Chaos* **18**, 2487–2642.

Cook, M. [2004] "Universality in elementary cellular automata," *Compl. Syst.* **15**, 1–40.

Freire, J. G. & Gallas, J. A. C. [2007] "Synchronization and predictability under rule 52, a cellular automaton reputedly of class 4," *Phys. Lett. A* **366**, 25–29.

Kitchens, B. [1998] *Symbolic Dynamics*: *One-Sided, Two-Sided and Countable State Markov Shifts* (Springer-Verlag, Berlin).

Martínez, G. J., Adamatzky, A., Alonso-Sanz, R. & Seck-Tuoh-Mora, J. C. [2010a] "Complex dynamic emerging in Rule 30 with majority memory," *Compl. Syst.* **18**, 345–365.

Martínez, G. J., Adamatzky, A., Seck-Tuoh-Mora, J. C. & Alonso-Sanz, R. [2010b] "How to make dull cellular automata complex by adding memory: Rule 126 case study," *Complexity* **15**, 34–49.

Martínez, G. J., Adamatzky, A. & Alonso-Sanz, R. [2013] "Designing complex dynamics in cellular automata with memory," *Int. J. Bifurcation and Chaos* **23**, 1330035-1–131.

Martínez, G. J., Adamatzky, A. & McIntosh, H. V. [2014] "Complete characterization of structure of Rule 54," *Compl. Syst.* **23**, 1–35.

Rendell, P. [2011] "A simple universal Turing machine for the game of life Turing machine," *J. Cell. Autom.* **6**, 323–340.

Rendell, P. [2013] "A fully universal Turing machine in Conway's game of life," *J. Cell. Autom.* **8**, 19–38.

Von-Neumann, J. [1966] *Theory of Self-Reproducing Automata* (University of Illinois Press, Urbana).

Wolfram, S. [1983] "Statistical mechanics of cellular automata," *Rev. Mod. Phys.* **55**, 601–644.

Wolfram, S. [1984] "Universality and complexity in cellular automata," *J. Phys. D*: *Appl. Phys.* **10**, 1–35.

Wolfram, S. [1986] *Theory and Applications of Cellular Automata* (World Scientific, Singapore).

Wolfram, S. [2002] *A New Kind of Science* (Wolfram Media, Champaign).

Zhou, Z. L. [1997] *Symbolic Dynamics* (Shanghai Scientific and Technological Education Publishing House, Shanghai).

Appendix A

The Properties of Remainder Gliders

In the following, the properties of remainder gliders are also presented.

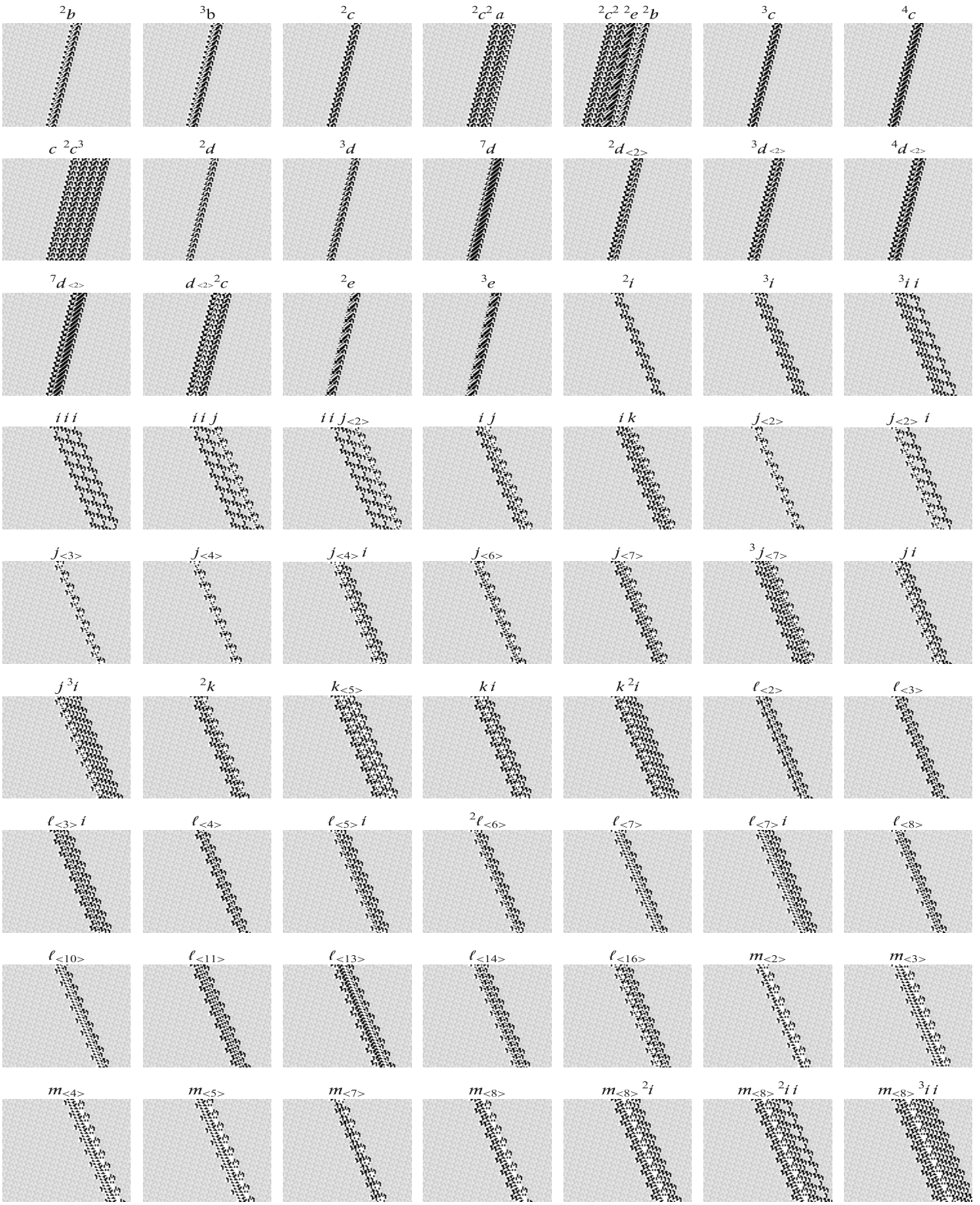

Fig. 11. The spatiotemporal patterns of other gliders.

Table 3. Characterizations of OGs and DCGs in Fig. 11.

Glider	Velocity	With	Glider	Velocity	With
^2b	$-1/5$	9–10	$j_{\langle 7\rangle}$	4/12	8–14
^3b	$-1/5$	10	$^3j_{\langle 7\rangle}$	4/12	13–19
^2c	$-1/5$	8	ji	4/12	11–15
$^2c^2\ ^2e\ ^2b$	$-1/5$	34–35	$j\ ^3i$	4/12	16–22
$^2c^2\ a$	$-1/5$	19–20	^2k	4/12	10–16
^3c	$-1/5$	8–9	$k_{\langle 5\rangle}$	4/12	16–22
^4c	$-1/5$	9–10	ki	4/12	11–17
$c\ ^2c^3$	$-1/5$	31–32	$k\ ^2i$	4/12	17–23
^2d	$-1/5$	6–7	$l_{\langle 2\rangle}$	4/12	7–13
^3d	$-1/5$	7–8	$l_{\langle 3\rangle}$	4/12	9–13
^7d	$-1/5$	10–11	$l_{\langle 3\rangle}\ i$	4/12	12–18
$^2d_{\langle 2\rangle}$	$-1/5$	9–10	$l_{\langle 4\rangle}$	4/12	7–13
$^3d_{\langle 2\rangle}$	$-1/5$	10–11	$l_{\langle 5\rangle}\ i$	4/12	9–15
$^4d_{\langle 2\rangle}$	$-1/5$	11–12	$^2l_{\langle 6\rangle}$	4/12	6–12
$^7d_{\langle 2\rangle}$	$-1/5$	13–14	$l_{\langle 7\rangle}$	4/12	8–14
$d_{\langle 2\rangle}\ ^2c$	$-1/5$	16–17	$l_{\langle 7\rangle}\ i$	4/12	14–20
^2e	$-2/10$	7–8	$l_{\langle 8\rangle}$	4/12	7–13
^3e	$-2/10$	7–8	$l_{\langle 10\rangle}$	4/12	9–13
^2i	4/12	6–12	$l_{\langle 11\rangle}$	4/12	11–17
^3i	4/12	9–15	$l_{\langle 13\rangle}$	4/12	14–20
$^3i\ i$	4/12	16–19	$l_{\langle 14\rangle}$	4/12	10–16
iii	4/12	17–23	$l_{\langle 16\rangle}$	4/12	12–16
iij	4/12	21–27	$m_{\langle 2\rangle}$	4/12	9–15
$iij_{\langle 2\rangle}$	4/12	19–25	$m_{\langle 3\rangle}$	4/12	10–16
ij	4/12	11–15	$m_{\langle 4\rangle}$	4/12	11–17
$i\ k$	4/12	13–19	$m_{\langle 5\rangle}$	4/12	11–15
$j_{\langle 2\rangle}$	4/12	5–11	$m_{\langle 7\rangle}$	4/12	7–13
$j_{\langle 2\rangle}\ i$	4/12	11–17	$m_{\langle 8\rangle}$	4/12	12–16
$j_{\langle 3\rangle}$	4/12	7	$m_{\langle 8\rangle}\ ^2i$	4/12	19–25
$j_{\langle 4\rangle}$	4/12	4–6	$m_{\langle 8\rangle}\ ^2i\ i$	4/12	28–32
$j_{\langle 4\rangle}\ i$	4/12	8–14	$m_{\langle 8\rangle}\ ^3i\ i$	4/12	29–35
$j_{\langle 6\rangle}$	4/12	7–13			

Table 4. Decimal expressions of glider factors in Fig. 11.

Glider Factor	With	Decimal Expression
$[^2b]$	22	(3453510/2922518/2368948)
$[^3b]$	42	(3612257890886/3061678888982/2486086067636)
$[^2c]$	40	(903064473158/765419721238/621521516980)
$[^2c^2\ ^2e\ ^2b]$	41	(1952973737542/1549335138838/1531654551988)
$[^2c^2\ a]$	39	(451513568838/382714647062/310759766452)
$[^3c]$	28	(220474950/186872342/151738804)
$[^4c]$	16	(60998/45590/47540)
$[c\ ^2c^3]$	32	(3527601734/2989978134/2427828660)
$[^2d]$	32	(3527595462/2989978134/2427818292)
$[^3d]$	20	(863686/730646/592180)
$[^7d]$	36	(56441531846/47838754326/38845102388)
$[^2d_{\langle 2\rangle}]$	16	(60998/44566/45492)
$[^3d_{\langle 2\rangle}]$	36	(56441530950/47838752278/38845100212)
$[^4d_{\langle 2\rangle}]$	24	(13823558/11693590/9482676)
$[^7d_{\langle 2\rangle}]$	20	(978502/749078/766388)
$[d_{\langle 2\rangle}\ ^2c]$	36	(56440925766/47839407638/38845239732)
$[^2e]$	27	(110236230/93436182/75869364)
$[^3e]$	15	(30278/23446/23988)
$[^2i]$	32	(3527595590/2989920790/2427818164)
$[^3i]$	16	(54854/45590/37044)
$[^3i\ i]$	32	(3527857734/2989928982/2427752628)
$[iii]$	48	(231184504377926/195947451036182/159109508075700)
$[iij]$	47	(115592245989958/97973716824598/79554743210164)
$[ii\ j_{\langle 2\rangle}]$	31	(1749209670/1486270998/1211470004)
$[ij]$	31	(1763725894/1494880790/1213895092)
$[i\ k]$	39	(451532214854/382709445142/310760542644)
$[j_{\langle 2\rangle}]$	31	(1763797702/1494960278/1213909044)
$[j_{\langle 2\rangle}\ i]$	23	(6890182/5835286/4774836)
$[j_{\langle 3\rangle}]$	39	(451532234822/382709858838/310760755380)
$[j_{\langle 4\rangle}]$	23	(6889542/5839382/4741812)
$[j_{\langle 4\rangle}\ i]$	39	(451532234822/382709864982/310760757940)
$[j_{\langle 6\rangle}]$	20	(860870/729238/590388)
$[j_{\langle 7\rangle}]$	20	(854086/726550/591284)

Table 4. (*Continued*)

Glider Factor	With	Decimal Expression
$[^3j_{\langle 7\rangle}]$	44	(14449031435846/12246715511318/9944343908532)
$[ji]$	31	(1763797062/1494964374/1213909044)
$[ji_{\langle 3\rangle}]$	47	(115592252190278/97973724468758/79554745615540)
$[^2k]$	23	(6886982/5833238/4722868)
$[k_{\langle 5\rangle}]$	41	(1806128193606/1530839368214/1243042959796)
$[ki]$	23	(6889542/5833238/4772276)
$[k\ ^2i]$	23	(6889542/4789782/4772276)
$[l_{\langle 2\rangle}]$	32	(3527590470/2989928982/2427823284)
$[l_{\langle 3\rangle}]$	29	(440948806/373741078/303478196)
$[l_{\langle 3\rangle}\ i]$	37	(112883025990/95677465110/77690181044)
$[l_{\langle 4\rangle}]$	45	(28898063078982/24493431112214/19888688509364)
$[l_{\langle 5\rangle}\ i]$	21	(1722438/1458838/1193524)
$[^2l_{\langle 6\rangle}]$	37	(112883058758/95677466262/77690189364)
$[l_{\langle 7\rangle}]$	40	(903064470214/765419721750/621521514676)
$[l_{\langle 7\rangle}\ i]$	40	(903064240838/765419722262/621521445044)
$[l_{\langle 8\rangle}]$	26	(55118534/46717078/37934644)
$[l_{\langle 10\rangle}]$	16	(49734/46614/41140)
$[l_{\langle 11\rangle}]$	18	(219206/185878/148916)
$[l_{\langle 13\rangle}]$	40	(903064487494/765419722262/621521451060)
$[l_{\langle 14\rangle}]$	42	(3612257880134/3061678888598/2486086059572)
$[l_{\langle 16\rangle}]$	28	(220472006/186866198/151722932)
$[m_{\langle 2\rangle}]$	16	(42054/44566/180)
$[m_{\langle 3\rangle}]$	35	(28220763846/23919329302/19422513332)
$[m_{\langle 4\rangle}]$	43	(7224477013574/6123351872022/4972139811252)
$[m_{\langle 5\rangle}]$	27	(110191174/93402646/75505844)
$[m_{\langle 7\rangle}]$	13	(4678/4246/1460)
$[m_{\langle 8\rangle}]$	32	(3527576646/2989917718/2427803060)
$[m_{\langle 8\rangle}\ ^2i]$	32	(3527576646/2987820566/2427803060)
$[m_{\langle 8\rangle}\ ^2i\ i]$	48	(231184437251142/195947985798678/159109491283380)
$[m_{\langle 8\rangle}\ ^3i\ i]$	48	(231184504456774/195947985658390/159105196241076)

Appendix B

Spatiotemporal Patterns of HCAM Rules

Several complex spatiotemporal patterns of some concrete HCAM rules are presented as follows:

HCAM(152,146)

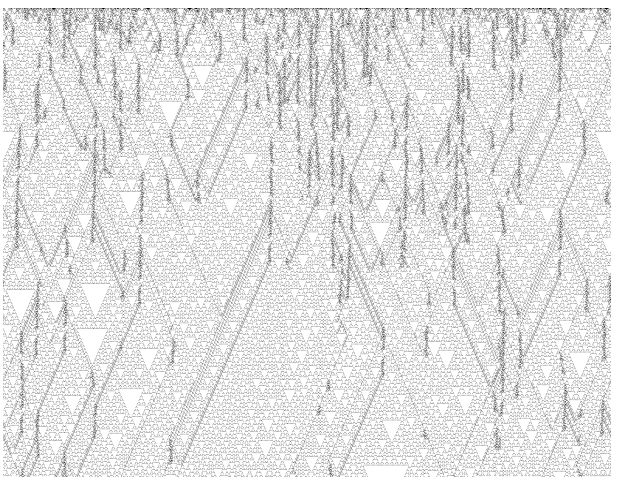

HCAM(232,146)

HCAM(6,30)

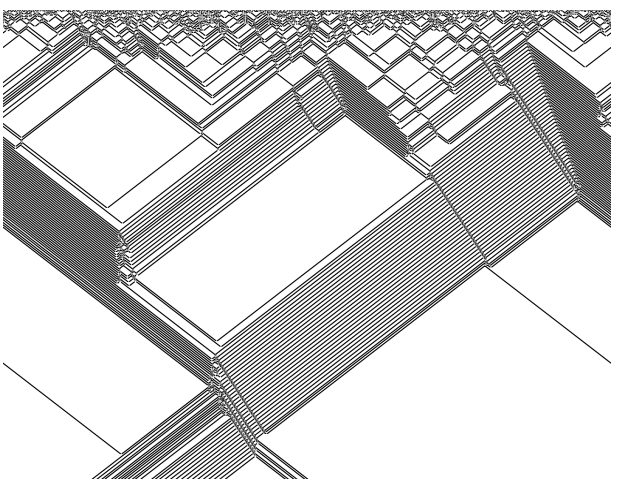

HCAM(44,178)

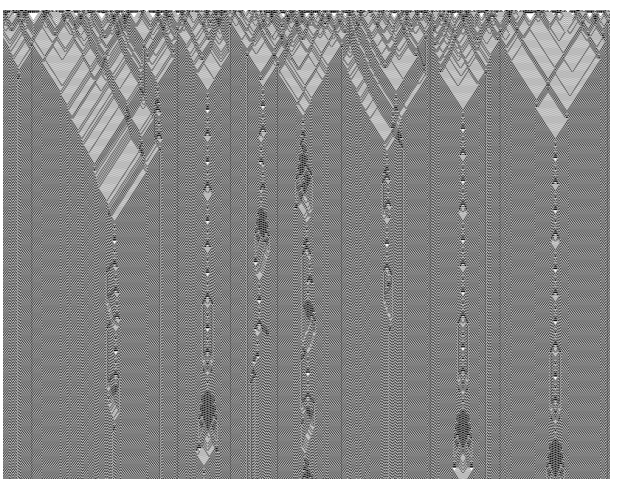

HCAM(11,129)

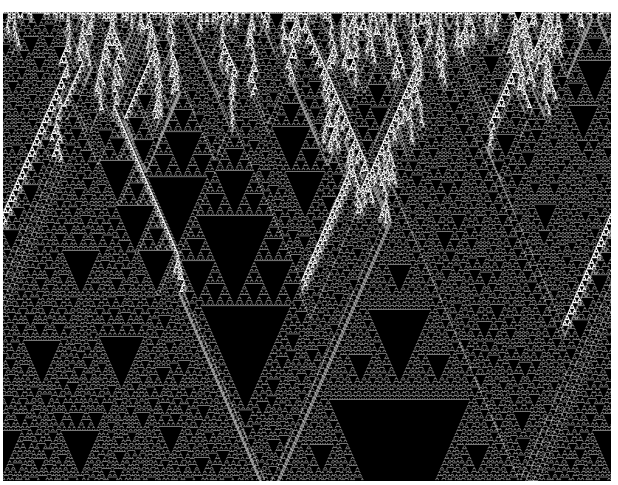

HCAM(129,57)

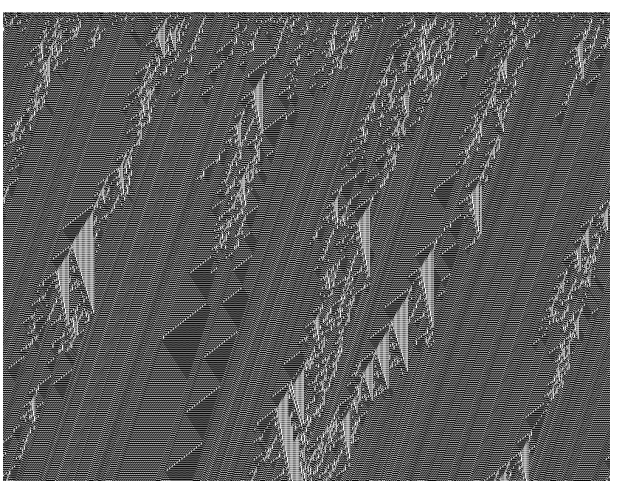

HCAM(10,133)

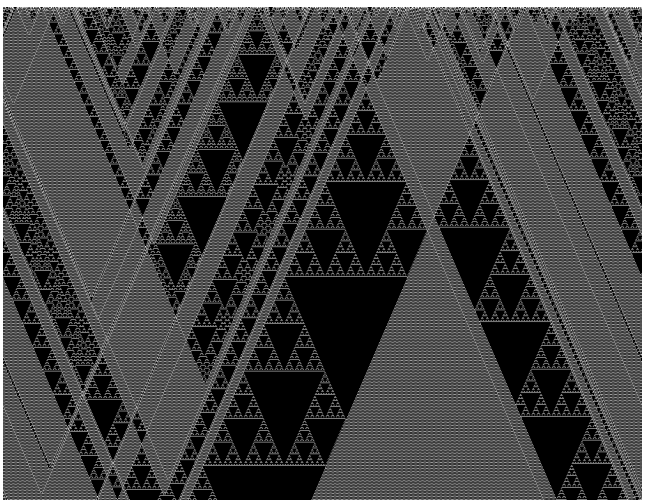

HCAM(14,37)

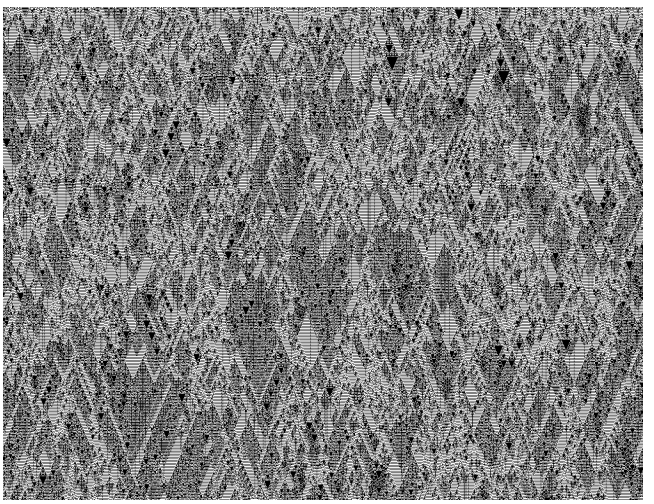

HCAM(22,6)

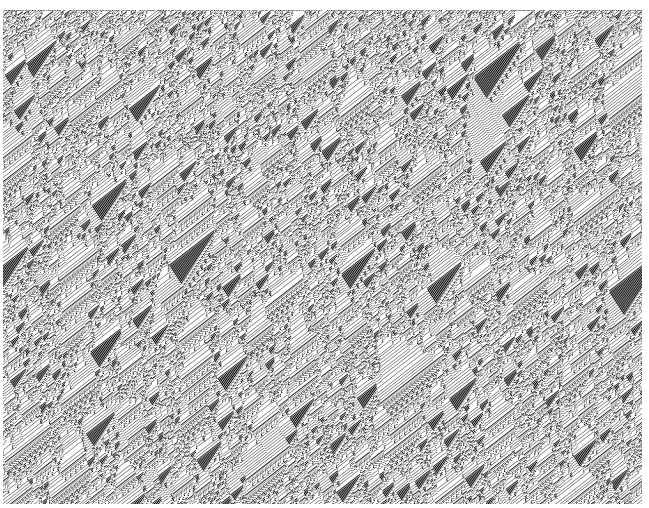

HCAM(28,5)

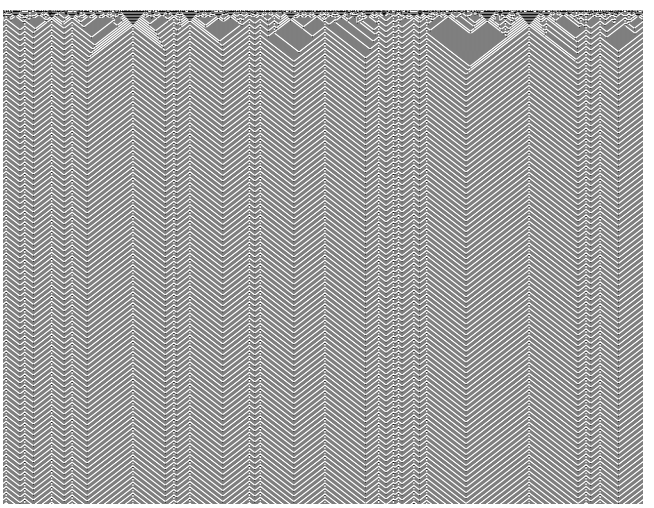

HCAM(28,46)

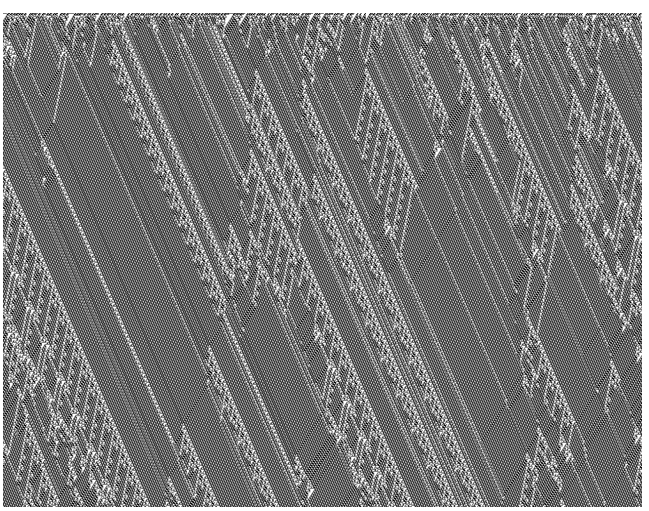

HCAM(28,133)

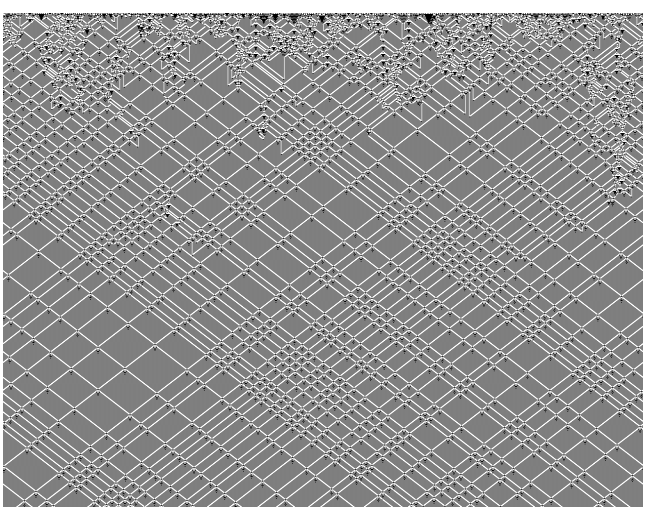

HCAM(42,133)

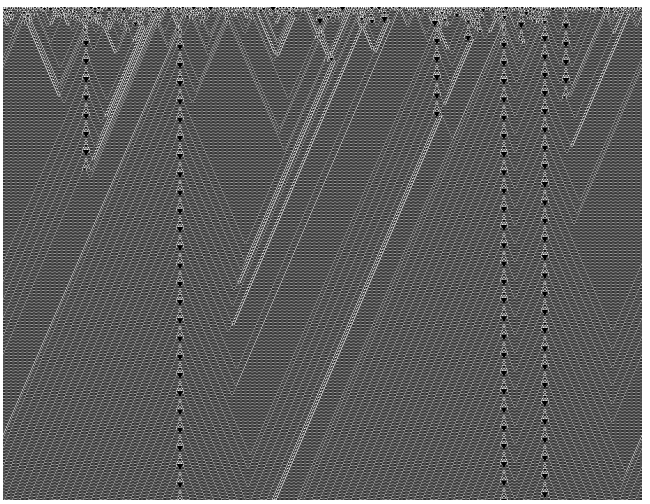

HCAM(50,74)

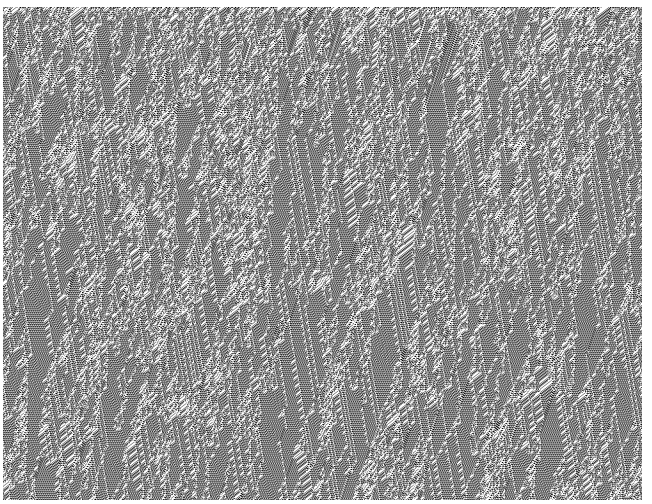

HCAM(50,166)

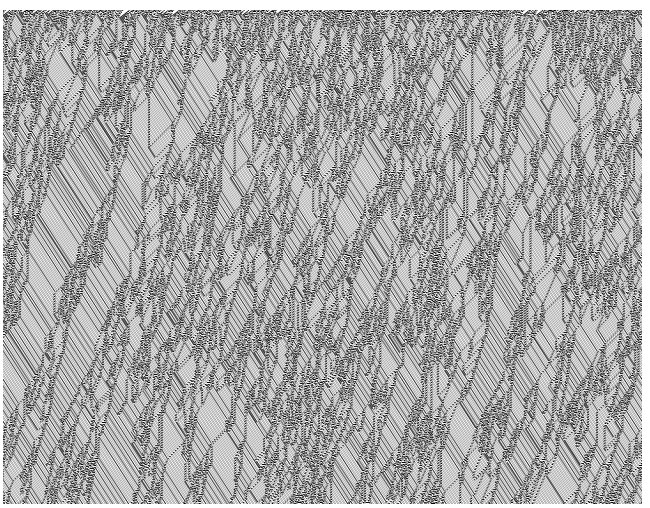

HCAM(54,9)

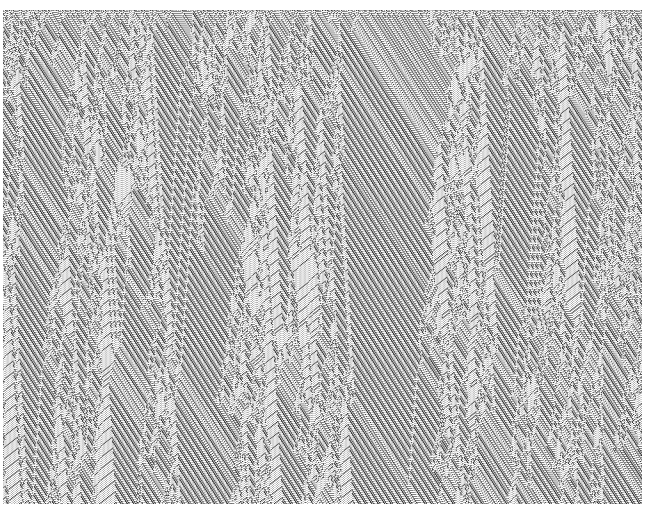

HCAM(54,110)

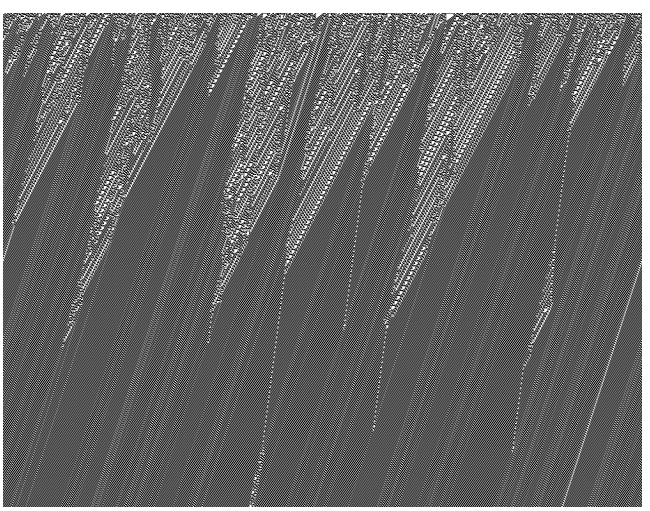

HCAM(56,45)

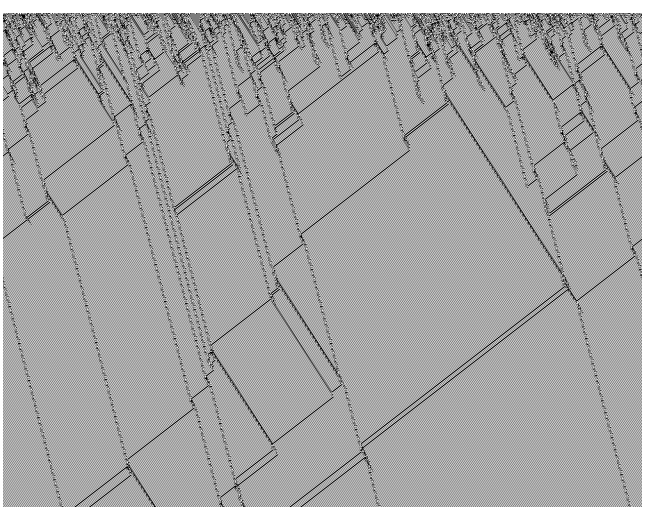

HCAM(73,29)

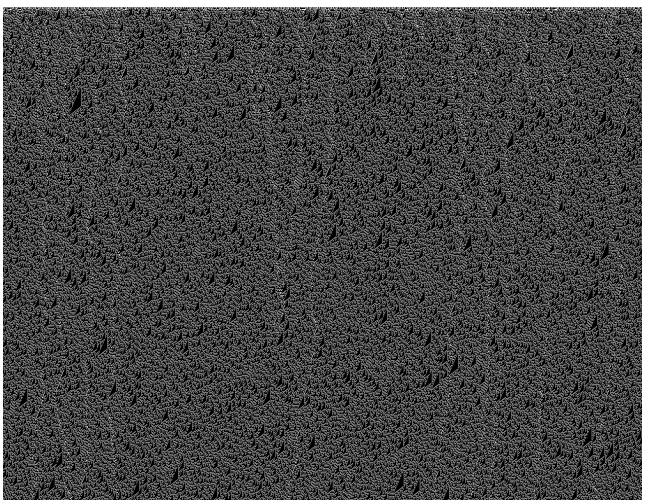

HCAM(74,178)

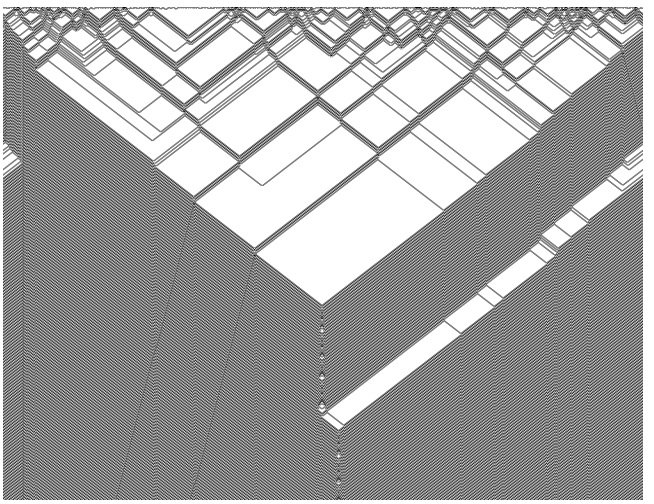

HCAM(90,178)

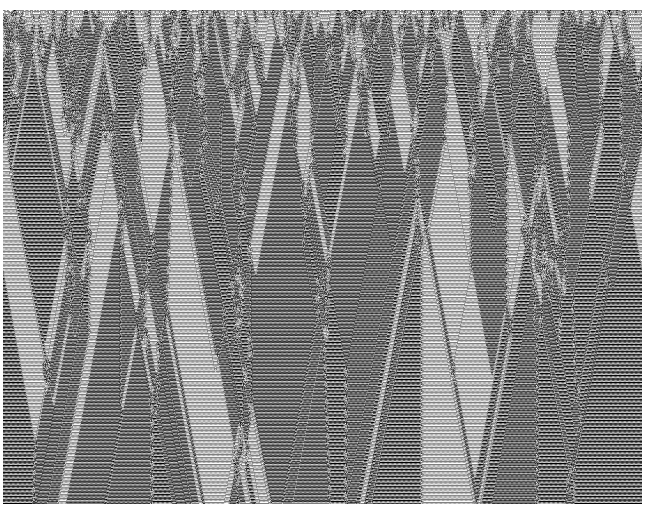

HCAM(138,110)

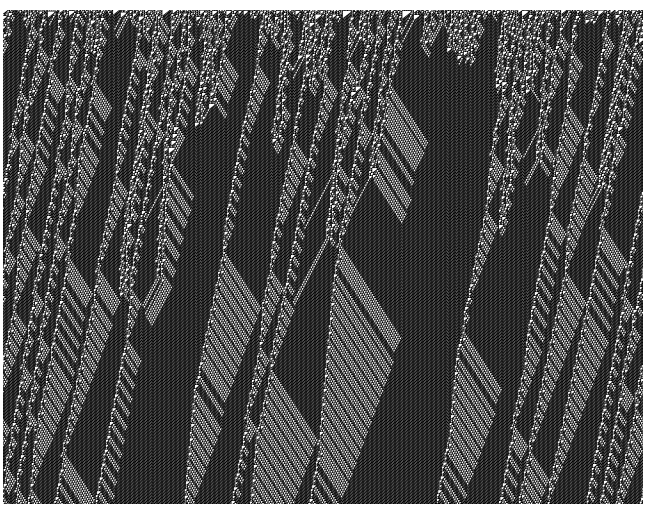

HCAM(146,38)

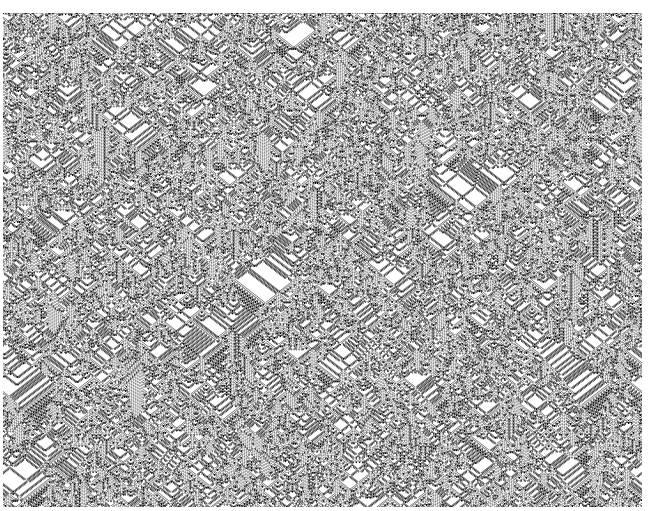

HCAM(146,110)

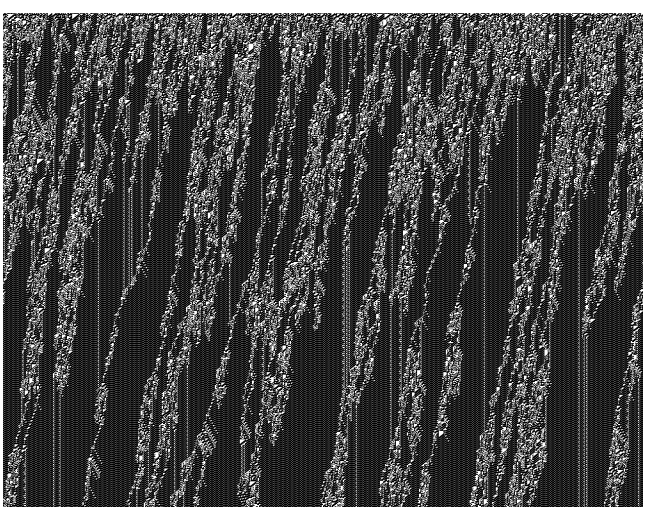

HCAM(178,74)

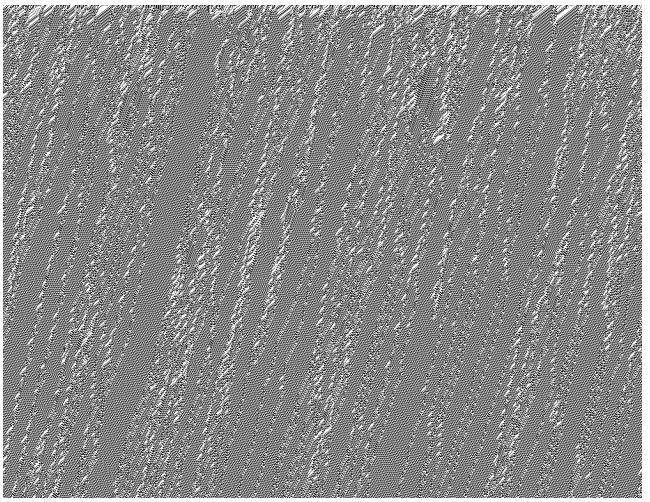

HCAM(178,110)